Journal of Chemical Health Risks
www.jchr.org
JCHR (2023) 13(5), 581-608 | ISSN:2251-6727

Role of Ionic Surfactants in Constitution of Binary Micellar System for Solubilizing Telmisartan

[1]E. Paul Raj, [2]Sutharsan karunanithi, [3]Puspalata Rajesh, [4]Sasmita Dash
[1,2,4] Department of Chemistry, Annamalai University, Annamalai Nagar, Tamil Nadu 608002, India.
[3] Water and Steam Chemistry Division, BARC Facilities, Kalpakkam, Tamil Nadu 603102, India.
[3] Homi Bhabha National Institute, Mumbai, Maharashtra 400094, India
*Corresponding author E-mail address: mishra342sas@gmail.com

(Received: 02 September 2023 Revised: 14 October Accepted: 07 November)

KEYWORDS
Solubilization, single micelle, binary polymeric micellar solution, Thermodynamic parameters, binding constant value.

ABSTRACT:
In this study, two binary micellar systems of Pluronic P-123 (P-123) were employed for solubilizing antihypertensive drug Telmisartan (TMS). They are, P123 with cationic surfactant, cetyl pyridinium bromide (CPB); and P123 with anionic surfactant, ammonium dodecyl sulfate (ADS). The solubilization studies in two polymeric binary micellar mediums were investigated through conductivity, FTIR, and UV-visible spectroscopy. The change in the particle size and charge were observed through SEM, dynamic light scattering, and zeta potential measurements. From the conductivity studies various thermodynamic parameters such as Gibb's free energy of micellization (ΔG_m), Enthalpy (ΔH_m), and entropy of micellization (ΔS_m) were calculated. There was a negative value of ΔG_m for both the mixed micellar systems, -20.4 kJmol^{-1} for CPB + P-123 + TMS and -25.9 kJmol^{-1} for ADS + P-123 + TMS. This is suggestive of the spontaneity of micellization of both the systems with drug TMS. UV studies demonstrated higher solubility with both the mixed micellar systems compared to solubilization in a single micelle of P-123. The binding constant values were determined from UV absorbance values using the Benesi - Hildebrand plot. The values were 79. 36 M^{-1} for TMS +P-123, 465.11 M-1 for TMS + P-123 + CPB and 1133.8 M^{-1} for TMS + P-123 + ADS. There was swelling of the micellar size from 16.23 nm to 52.02 nm for CPB group and from 3.16 nm to 32.04 nm for ADS group due to the encapsulation of TMS in the mixed micellar cavities. Size of both the ternary systems containing drug are suitable for cellular uptake. This study offers two alternative combinations of mixed polymeric micellar systems to enhance TMS solubilization to improve bioavailability.

Highlights

- Better solubilization of TMS can be achieved through a binary micellar medium than a single micellar one.
- For constituting a binary micellar solution for TMS, ADS is more suitable than CPB.
- This study offers a novel combination for TMS with greater solubility and bioavailability.

Introduction

Overcoming drug insolubility through combinatorial chemistry is gaining importance in recent years. Approximately 40% of the new active pharmaceutical ingredients are known to have good pharmacological activity. But they have poor aqueous solubility resulting in low bioavailability [1]. Drug solubility in biological fluid and its concentration to an acceptable degree in any

Journal of Chemical Health Risks

www.jchr.org

JCHR (2023) 13(5), 581-608 | ISSN:2251-6727

physiological system is important for producing the requisite drug effect in the human body. The primary condition for these pharmacological effects is that the drug should be soluble in the biological fluid. Hence, it is necessary to tune the environment of the drug in such a way that it is consistently soluble giving a required biological impact.

According to the biopharmaceutical classification system (BCS) the insoluble drugs are classified as class II drugs. These drugs have less aqueous solubility and high permeability [2]. Many methods are adopted such as solid dispersion, micro ionization, complexation, change of pH, and micellar solubilization [3,4]. Among the above methods, micellar solubilization is preferred as a drug carrier for many drugs due to their smaller particle size, nontoxicity, controlled release, enhanced permeability, and longer residence time in the system. It is used extensively for the treatment of essential hypertension [5]. The chemical name of Telmisartan (TMS) is 4'-[(1,4'-dimethyl-2'-biphenyl[2,6'-bi-1H-benzimidazol]-1'-yl)methyl[1,1'-biphenyl]-2-carboxylic acid [6]. It has a long half-life (24 h) when compared with other angiotensin II receptor blockers. One important property of this drug is its high lipophilicity. Because of this, there is more effective distribution and better tissue penetration of the drug [7]. However, one of the major concerns of TMS is that it is poorly soluble in aqueous medium, hence, in biological fluids also its solubility is limited [8]. There have been many successful attempts to enhance TMS solubility. But some are expensive and multistep processes [9], and some have instability problems [5]. Many drugs available in the market are in solid dispersion form [10]. Numerous surfactant systems are used for effective drug targeting and controlled release [11,12]. In some cases, the solid dispersion forms are tuned for better efficacy by the addition of surfactants. Micellar solubilization of hydrophobic drugs is commonly used in the pharmaceutical industry. In the category of surfactants, the Pluronic group is preferred because of their lower critical micellar concentration (CMC), better solubility, and controlled drug release. The Pluronic group of tri-block polymers either in a single form or in binary are prepared and used for various drugs. A poorly soluble drug like carbamazepine is solubilized in Pluronic [13]. They are also used as solubilizers for anticancer drugs [14]. There are uses of Pluronic P-123 as solubilizers in curcumin [15], paclitaxel [16], and docetaxel [17]. Pluronic P-123 and Pluronic F-127 have been used in solubilizing TMS [18–20]. Mixed micellar have been used for efficient solubilization of hydrophobic drugs [21-24]. There are a few studies on solubilization and interactions of a few drugs with various micellar systems of sodium dodecyl sulfate (SDS) and CPB by different research groups [25-27]. However, there is no work reported for ADS as a drug solubilizer. Also, binary micellar solution of P-123 with ionic surfactants to solubilize TMS is not available.

The CMC of surfactants are the deciding factor for the solubilization of hydrophobic drugs. And, the CMC of Pluronic is highly dependent and sensitive to the change in temperature [28]. The Pluronic group of amphiphiles generally form spherical micelles, wherein the hydrophobic part (PPO blocks) are at the core surrounded by the hydrophilic part (PEO blocks) at the corona [29]. These micelles are capable of organizing into cubic structures to generate thick and non-transparent gels above ~20% polymers. In this work, Pluronic micellar solution is used at a post-CMC concentration. Attempts have been made to tune the P-123 surfactant by combining it with a cationic surfactant, Cetyl Pyridinium Bromide (CPB) and an anionic surfactant, Ammonium Dodecyl Sulfate (ADS), for improving some physico chemical properties while interacting with drug TMS. The investigations were done through conductivity, UV-Spectrophotometry, FTIR, DLS, Zeta potential, and SEM studies. The impact of the positive and negative charges on the constitution of binary micellar systems using P-123 was assessed while solubilizing TMS.

2. Materials and Methods:

Pluronic P-123 (95 % purity), CPB (97 % purity), and ADS (98 % purity) used were as sigma Aldrich grade. TMS (97 % purity) was supplied by Madras Pharmaceutical Ltd. It was used without further purification. Double distilled water was used for solution preparation.

2.1. Sample Preparations:

Stock solutions of TMS were prepared by weighing 0.0106 g in 20 ml of methanol. To this 80 ml of pH 7.4 (phosphate buffer) was added and the volume was made up

Journal of Chemical Health Risks
www.jchr.org
JCHR (2023) 13(5), 581-608 | ISSN:2251-6727

to 100 ml. The concentration of the stock solution was 20.59 μM. For different experiments, this stock solution was diluted suitably.

The stock solution of 20 mM CPB surfactant was prepared by weighing 0.8 g in 100 ml double distilled water. After that, it was sonicated for 20 minutes to get a transparent solution.

About 1.8 g of the anionic surfactant ADS was weighed accurately and dissolved in 100 ml double distilled water at room temperature. The prepared stock solution was of 60 mM concentration.

Pluronic P-123 solution was prepared by weighing accurately 5 g of stock solution. It was dissolved in 10 ml of double distilled water and then kept in the refrigerator for 24 hours. Then it was made up to 100 ml. The stock solution concentration was 8.716 mM which was suitably diluted for different experiments.

Methods:

2.2. Conductivity Measurement:

The conductance of the TMS solution in the presence of two mixed micellar solutions viz., P-123 + CPB and P-123 + ADS was observed through conductivity measurements. They were compared with the conductance of both the pure ionic surfactants, CPB and ADS. The experiments were carried out using a PICCO–180 conductivity meter assembled with a platinum electrode dipped in the solution. All the measurements were done at room temperature. Calibration was carried out before starting the experiment using a standard potassium chloride solution. The chosen concentrations of surfactants were before, at, and after CMC. The measured specific conductance values were plotted against the concentration of the surfactants. From the plots, after identifying CMC, which is the point of inflection, the pre- and post-micellar slopes were determined. From the slopes, the counter ion binding constant β was calculated using the formula,

$\frac{S_1}{S_2} = \alpha$--- (1)

$1-\alpha = \beta$-- (2)

Where S_1 and S_2 represent the slopes of post and premicellar concentration respectively. Define α. Using β, various thermodynamic parameters like ΔG, ΔH, and ΔS were calculated using the formula,

$\Delta G = (2-\beta)\, RT \ln X_{cmc}$--- (3)

where T is the temperature, X_{cmc} is the mole fraction of surfactant and R is the gas constant = 8.314 J/mol k

$\Delta H = -2.3\,(2-\beta)\, RT2 \left[\frac{\partial\,(\log Xcmc)}{\partial\, T}\right]_{\rho}$-------------------------- (4)

From the above equation, plotting log X_{cmc} vs. T gives a straight line with a slope (log X_{cmc})/ƏT. The entropy was obtained by using the formula,

$\Delta S = \frac{\Delta H - \Delta G}{T}$ --- (5)

2.3. Fourier transform infrared spectrum:

The FTIR spectra of TMS, TMS in the presence of single/mixed surfactants were recorded using carry–630 FTIR, Agilent technologies. The spectra were recorded in the range of 600 to 4000 cm^{-1}. There were four samples used for the experiment. TMS, TMS + P-123, TMS + P-123 + CPB and TMS + P-123 +ADS. Except first one, the other three samples were taken in a 1:1 ratio, and ground in a mortar for uniformity before taking the runs. The structural changes occurring in TMS in the presence of single/binary micelles were noted. The chemical structures of TMS and surfactants are displayed in Fig.1

2.4. UV spectrophotometry:

UV spectrophotometric studies were carried out using Shimadzu UV – 2600K with a 1 cm quartz cell. From the stock solutions, suitable dilutions were made and three sets of readings were recorded. They were TMS + P-123, TMS + P-123 + CPB and TMS + P-123 + ADS.

The binding constant K_b was calculated from the UV absorption data using a Benesi-Hildebrand plot using the formula:

$A = (A_0 + B\, K_b\, C)/ (1 + K_b\, C)$ ------------------------------- (6)

where,

A_0= Absorbance of pure probe TMS in P-123

A= Absorbance of analyte at different concentrations of CPB or ADS

B= Constant

C= Surfactant (CPB or ADS) concentration (M)

2.5. Zeta Potential:

Journal of Chemical Health Risks
www.jchr.org
JCHR (2023) 13(5), 581-608 | ISSN:2251-6727

The zeta potential of two ionic surfactants viz., CPB, ADS, and their mixed micelles with P-123, viz., P-123 + CPB and P-123 + ADS) without and with TMS were monitored. The instrument used was a Nano–ZS Zetasizer from Malvern panalytical, UK. Manual measurement mode was used. Each sample was measured three times with 15 runs in each measurement with disposable folded capillary cells.

2.6. Dynamic light scattering (DLS) Studies:

The micellar size of the single/mixed micellar systems without and with TMS was measured by dynamic light scattering correlation spectroscopy using Nano – ZS Zetasizer from Malvern Panalytical, UK at 25 ºC. Manual measurement mode was used. Each sample was measured three times with 15 runs in each measurement with disposable folded capillary cells from the change in the micellar size, the drug encapsulation in different micellar systems was assessed and analyzed. All analysis assumed spherical micelle formation (which may not always comply with reality) for relative comparisons.

2.7. Scanning electron Microscopy (SEM) studies:

Scanning electron microscopic (SEM) images were taken to study the morphological information about the sample surface. The instrument used was JSM-6610 LV. The observation maximum of the sample was up to 5 µm diameter. At 30 KV, the high-resolution measurement showed clarity with fine structure. The images were taken for TMS, TMS + P-123, TMS + P-123 + CPB, and TMS + P-123 + ADS. They were recorded for two different magnifications.

3. Results and discussion:

3.1. Conductivity studies:

The structure of the drug telmisartan (TMS) and the three surfactants; Pluronic P-123, cetyl pyridinium bromide (CPB), and ammonium dodecyl sulfate (ADS) are presented in Fig 1.

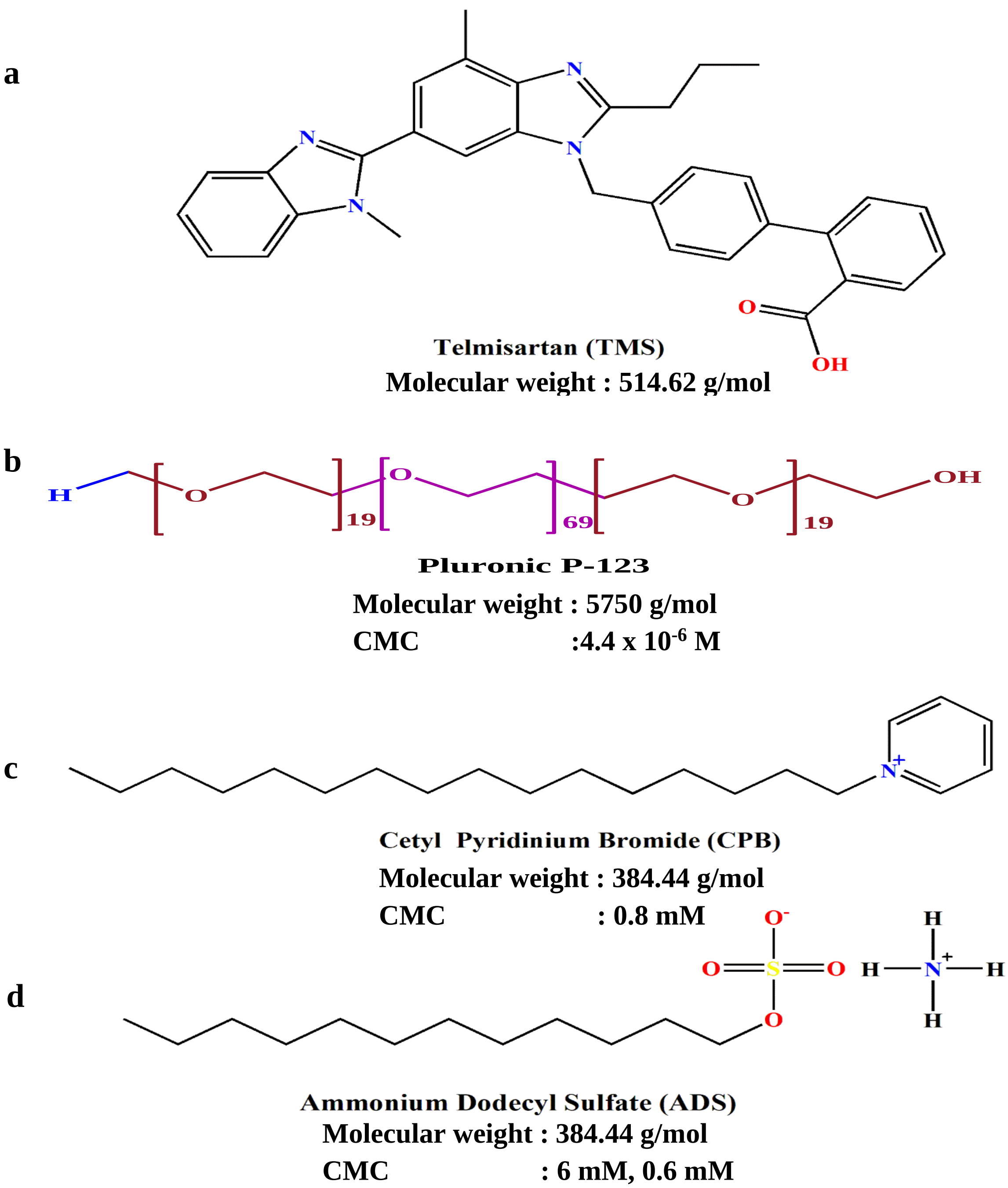

Fig 1. The structures of **(a)** drug Telmisartan **(b)** Pluronic P-123 **(c)** Cetyl Pyridinium Bromide and **(d)** Ammonium Dodecyl Sulfate.

Journal of Chemical Health Risks

www.jchr.org

JCHR (2023) 13(5), 581-608 | ISSN:2251-6727

The ionic surfactants behave like electrolytes in aqueous medium. Hence, the aggregation properties of CPB and ADS in presence of P-123 in the first step to form mixed micelle and in the next step, the interaction of mixed micelle with TMS was studied. Conductivity studies on these micelles in different systems are reported in the literature [30-38]. Pristine CPB was taken in different concentrations. The specific conductivity values were recorded and plotted against concentration. From the sharp change of specific conductance, (shown in Fig 2 a) the CMC value was evaluated. It was observed to be 0.8 mM which is in good agreement with the reported literature values of 6.0×10^{-4}M [27], 7.3×10^{-4}M [39], 7.1×10^{-4}M [40], 0.76 mM [41]. In the next step, P-123, the nonionic surfactant was added to the same concentrations of CPB as before. Although the ionic contribution for conductance was minimum, the mixed micelle of CPB + P-123 showed somewhat higher conductance values. The point of intersection was 0.5 mM which is the CMC (Fig 2 (b)). The CMC thus reduced from 0.6 mM (pure CPB) to 0.5 mM for mixed micelle indicating that the latter is a better solubilizing medium. The following step was to add a fixed concentration of TMS into the mixed micellar system of CPB + P-123. The CMC of this system was observed (shown in Fig 2 c) to be 0.4 mM, further lower a value than the mixed micelle. Hence, it can be predicted that the mixed micelle P-123 + CPB solubilized the drug TMS successfully. Similar lowering of CMC by previous researchers during drug solubilization have been reported before [42].

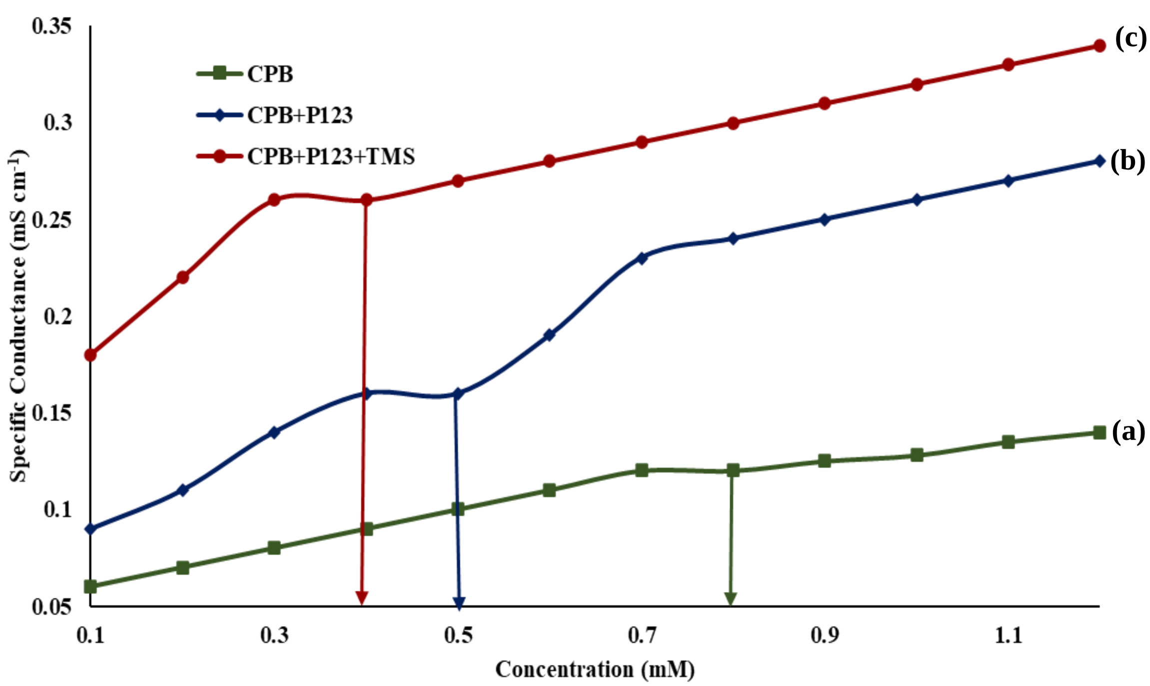

Fig 2. Specific conductivity of **(a)** CPB **(b)** CPB + Pluronic P-123 and **(c)** CPB + Pluronic P-123 + Telmisartan.

In a similar fashion, ADS, the anionic surfactant was taken in different concentrations. The specific conductance values were noted and plotted against the concentration. Here too, the point of sharp increase was observed at 6 mM, which was assigned to be the CMC (Fig 3 a). The value matches with reported literature values of 6.48 mM [34], 6.16 mM [36], 6.5 mM [38]. In the succeeding step, nonionic P-123 was added and conductance was monitored. The CMC was observed to be 4.8 mM for ADS + P-123 (Fig 3 b). Thus, this can also be predicted to

Journal of Chemical Health Risks
www.jchr.org
JCHR (2023) 13(5), 581-608 | ISSN:2251-6727

be a successful mixed micellar system. The next step was to add the drug TMS to the mixed micelle at different concentrations of the ADS. The CMC was found to be 3.6 mM (Fig 3 c), still lower a value than ADS + P-123. Thus, it can be said that TMS has been successfully solubilized in the ADS + P-123 medium. It is apparent that there is increased specific conductance as one moves from ionic surfactant to ionic surfactant – P123-TMS. Fig 2 and fig 3 display this. It is noteworthy to mention that in fig 2 and 3 there are some points with same specific conductance value. In such a case, the most prominent break is presumed as the CMC.

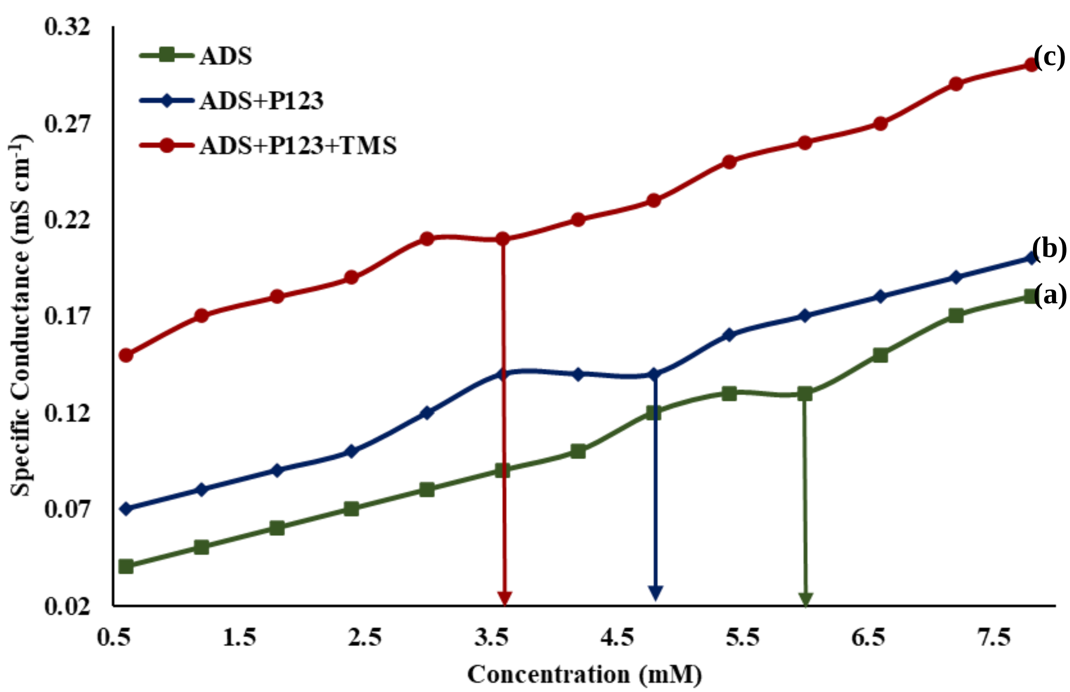

Fig 3. Specific conductivity of **(a)** ADS **(b)** ADS + Pluronic P-123 and **(c).** ADS + Pluronic P-123 + Telmisartan.

3.1.1. Calculation of thermodynamic parameters:

After identifying the CMC of the cationic and anionic sets of surfactants, in the presence and absence of TMS, the slopes of the premicellar and post micellar regions were found. From the slopes, S1 and S2, the counterion binding constant β and various thermodynamic parameters were calculated using the formula described in 2.2. The results are shown in Table 1 along with other reported literature values.

In the CPB set, the ΔG, Gibbs free energy of micellization was found to be -13.76 kJ mol^{-1}. The second aliquot, CPB + P-123 showed -19.18 kJ $mol^{-1,}$ and third aliquot, CPB + P-123 + TMS displayed -20.4 kJ mol^{-1}. The negative value in all three cases is a sign of the occurrence of spontaneous micellization. And, higher negative value of -20.4 kJ mol^{-1} of the TMS mixed micellar system compared to CPB and CPB + P-123 indicated the formation of a stable complex (CPB + P-123 + TMS) with greater spontaneity. The ΔH were found to be -5.7 kJ mol^{-1}, -6.4 kJ mol^{-1}, and -9.8 kJ mol^{-1} for the above-said systems. The negative values here indicate that the micellization is exothermic for the three systems. The ΔS entropy of micellization, values for the three aliquots were 3.3 kJ mol^{-1}, 4.2 kJ mol^{-1}, and 3.5 kJ mol^{-1} respectively. The positive value of ΔS is symbolic

Journal of Chemical Health Risks

www.jchr.org

JCHR (2023) 13(5), 581-608 | ISSN:2251-6727

of more disorderness developed in the system. Hence, the micellization is favorable for the solubilization of TMS.

In the ADS set, the free energy of micellization ΔG was -6.3 kJmol^{-1} for pristine ADS, -16.0 kJ mol^{-1} for ADS + P-123, and -25.9 kJ mol^{-1} for ADS + P-123 + TMS. All three negative values suggest spontaneity of micellization and the highest negative value for the third aliquot predicts that the solubilization of TMS is more spontaneous. The ΔH values were -2.8 kJ mol^{-1}, -6.8 kJ mol^{-1}, and -10.6 kJ mol^{-1}, respectively for the three sets. This suggests that the micellization is exothermic in nature. The ΔS values observed were 1.11 kJ mol^{-1}, 3.0 kJ mol^{-1}, and 5.3 kJ mol^{-1} respectively. The positive values infer that the three systems are entropy driven and the highest value of 5.3 kJ mol^{-1} among the three systems indicated greater stability of the ADS + P-123 + TMS system. There are some previous works reported by different research groups. The ΔG, ΔH, and ΔS values of all the literatures are presented in Table 1. The methods and systems are also mentioned in the table. The discrepancy observed for ΔG, ΔH, and ΔS from our data may be due to the difference in the medium of micellization reported in the literature [30,32-34].

Table 1. Thermodynamic parameters of Telmisartan in the ionic and non-ionic mixed micellar systems at different chemical environments were collected from literature with results from this work.

System	Temp (K)	ΔG kJ mol^{-1}	ΔH kJ mol^{-1}	ΔS kJ mol^{-1}	Ref
CPB with 1 mM buffer solution at pH 7.3 as observed from ITC studies	25^0C	-12979.6 kcal mol^{-1}	-2937 kcal mol^{-1}	33.7 kcal mol^{-1}	[30]
	30^0C	-14278.8 kcal mol^{-1}	-3189 kcal mol^{-1}	36.6 kcal mol^{-1}	
	35^0C	16076.4 kcal mol^{-1}	-4280 kcal mol^{-1}	38.3 kcal mol^{-1}	
	40^0C	17133.2 kcal mol^{-1}	-5114 kcal mol^{-1}	38.4 kcal mol^{-1}	
CPB in aqueous solutions of DMSO		**kJ mol^{-1}**	**kJ mol^{-1}**	**kJ mol^{-1}**	[32]
		-47.46	24.58		
		-48.84	14.20		
		-42.35	-14.65		
		-42.53	-13.16		
		-33.34	13.23		
CPB in aqueous solutions of DESO		-48.51	-12.57		
		-45.39	-19.73		
		-44.11	-20.53		
		-41.52	-22.57		
		-40.41	25.19		
CPB in Various Compositions of PrOH− WR Mixed Media	298.15 K	-46.63	30.36	0.258	[33]
		-44.13	12.30	0.189	
		-42.14	-	-	
		-43.38	-25.20	0.061	
		-39.16	-	-	
		-37.29	-18.82	0.062	
		34.29	-	-	
		32.07	20.85	0.038	
		32.38	-	-	
	303.15 K	-46.41	30.81	0.255	
		-44.75	12.59	0.189	
		-42.09	-25.07	0.056	

		-38.87	-20.03	0.062	
		-32.60	-21.80	0.036	
Micellization of ADS	24^0C	-18.371	-1.194	0.058	[34]
	29^0C	-17.430	-2.471	0.050	
	34^0C	-18.448	-3.966	0.047	
CPB	300 K	-13.766±0.068	-5.736±0.065	3.343±0.625	[This work]
CPB + P-123	300 K	-19.184±0.050	-6.425±0.074	4.253±0.621	
CPB + P-123 + TMS	300 K	-20.416±0.042	-9.803±0.046	3.537±0.761	
ADS	300 K	-6.381±0.036	-2.868±0.074	1.117±0.063	
ADS + P-123	300 K	-16.004±0.032	-6.895±0.087	3.036±0.751	
ADS + P-123 + TMS	300 K	-25.959±0.041	-10.612±0.451	5.398±0.065	

3.2. FTIR Spectroscopy:

The structural changes in drug TMS due to the addition of single and binary micelles were observed through FTIR studies. The FTIR of TMS is well studied by researchers [19,43-60]. The bond assignments of our results are displayed in Table 2 and Figure 4. In Table 3, the IR spectra observed for TMS by different groups of scientists in various chemical environments are also presented.

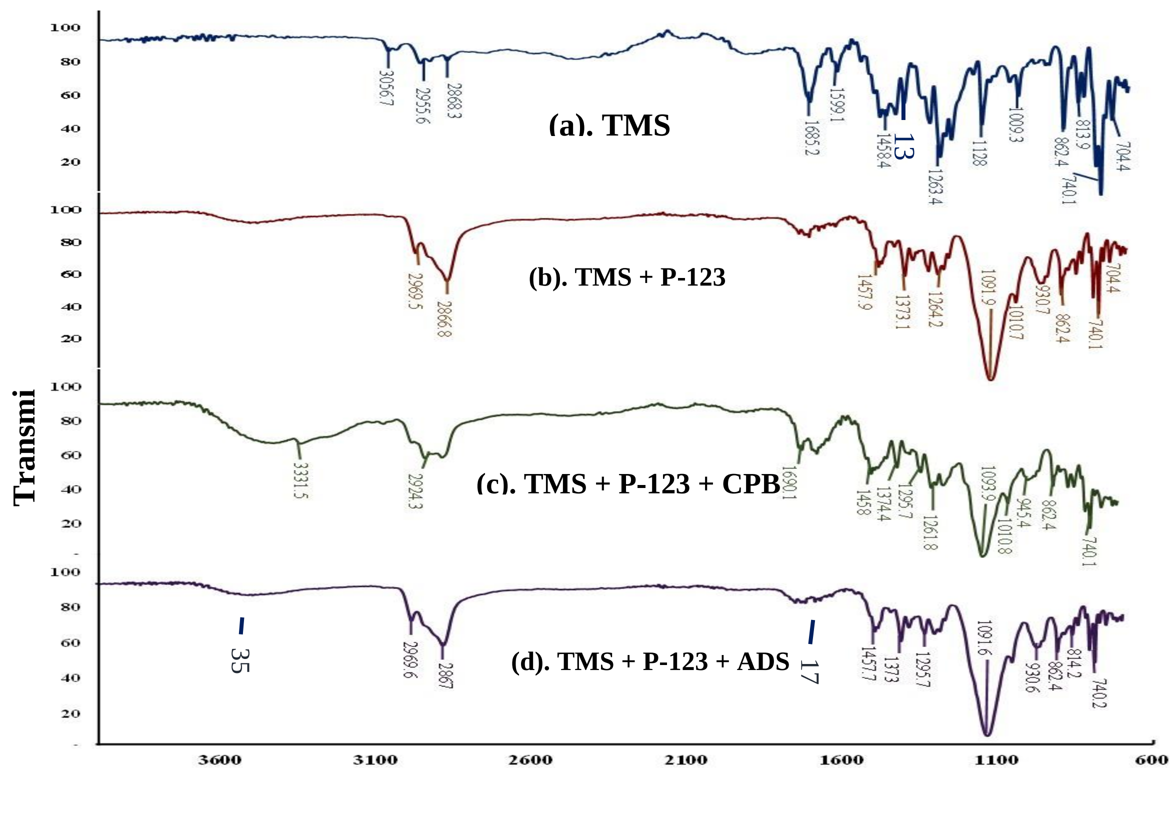

Fig 4. IR spectra of **(a).** TMS, **(b).** TMS + P-123, **(c).** TMS + P-123 + CPB, **(d).** TMS + P-123 + ADS

Journal of Chemical Health Risks

www.jchr.org

JCHR (2023) 13(5), 581-608 | ISSN:2251-6727

Table 2. The IR spectrum of **(i)** TMS, **(ii)** TMS + P-123, **(iii)** TMS +P-123 + ADS, **(iv)** TMS + P-123 + CPB

Assignments	Wavenumber (cm^{-1})			
	TMS	**TMS+P-123**	**TMS+P-123+CPB**	**TMS+P-123+ADS**
N-H stretching	3056	-	3566	3529
C-H stretching	2955	2969	2969	-
O-H stretching	2868	2866	2867	3529, 2924, 2868
C=C stretching	1599, 1685	1695	1717	1690
C-N stretching	1380, 1128, 1009	1373, 1091	1373	1374
C-O stretching	1263, 1128,	1295, 1264, 1091	1295, 1264, 1091	1295, 1261, 1093
C=C bending	862, 813	862, 813	930, 862, 814	1010, 862
C-H bending	1458	1457, 740	1457, 740	1458, 740

Table 3. IR spectra of Telmisartan in different chemical environments collected from the literature.

	N-H stretching	**O-H stretching**	**C=C stretching**	**C-N stretching**	**C-H bending**	***Ref***
Telmisartan wavenumber (cm^{-1})	2959, 2931	2871	1733, 1616		758, 741	[19]
	3416, 2965		1695, 1604	1396, 1267	1452, 740	[43]
	3416, 2962		1698	1350 - 1200	1460	[52]
	3375, 2933	2871	1698			[53]
	3421, 2933	2869	1962, 1613, 1599			[54]
	3022		1702, 1571		749	[55]
		2867	1698	1267	1458	[56]
	3446, 3063, 2957		1697, 1599		1458	[57]
	3443		1733, 1694			[58]
			1699		758, 740	[59]
	3433		1690, 1579			[60]
	3450, 2900		1600	1385, 1350, 1210		[44]
	3433, 3057, 2958		1695, 1603		1455	[45]
	3410, 3056, 2957		1598	1382	1459	[46]
	3500 - 3300	3000 - 2800	1693		757	[47]
	3057, 2960		1701, 1608	1334	738	[48]
	3445		1614, 1599			[49]
	3060		1692			[50]
	3063, 2957		1695, 1604	1303, 1236	1454	[51]
	3056, 2955	2868	1599, 1685	1380, 1128, 1009	1458, 740	[This work]

Journal of Chemical Health Risks

www.jchr.org

JCHR (2023) 13(5), 581-608 | ISSN:2251-6727

For TMS, there were bands at 3056 cm^{-1} for N-H stretching, 2955 cm^{-1} for C-H stretching, 2868 cm^{-1} for O-H stretching, 1599 cm^{-1} and 1685 cm^{-1} for C=C stretching, 1263 cm^{-1} for C=O stretching, 862 cm^{-1} and 813 cm^{-1} for C=C bending, 1458 and 740 cm^{-1} for C-H bending. All these signals match the literature. In addition of P-123 to TMS there were peaks at 2965 cm^{-1}, 2866 cm^{-1}, 1457 cm^{-1} 740 cm^{-1} they stand for C-H stretching, O-H stretching and C-H bending, respectively. There were also signals at 1373 cm^{-1}, 1264 cm^{-1}, 1091 cm^{-1}, and 862 cm^{-1} which were due to C-N stretching and C=C bending, respectively. 1128 cm^{-1} of TMS gets shifted to lower wave number 1091 for C-N stretching with a high intensity predicting that there is bond formation. The 2868 cm^{-1} band shifts to 2866 cm^{-1}, and another shift to a lower number infers a short and strong bond in the area.

The next sample was with TMS + P-123 + CPB. Here, signals observed were at around 3331 cm^{-1}, 2924 cm^{-1}, and 2868 cm^{-1} which were due to O-H stretching frequency. There were also bands at 1690 cm^{-1}, and 1374 cm^{-1} representative of C=C stretching and C-N stretching respectively. Peaks at 1295 cm^{-1}, 1261 cm^{-1}, and 1093 cm^{-1} are symbolic of C-O stretching frequency. The strong peak at 1010 cm^{-1}, 862 cm^{-1} is for C=C bending and 1458 cm^{-1}, 740 cm^{-1} for C-H bending. The 1599 cm^{-1} of TMS gets shifted to a lower wave number of 1458 cm^{-1} due to bond formation in this area. The 1128 cm^{-1} of TMS gets shifted to a lower wave number at 1093 cm^{-1} predicting that at C-O stretching area, there is bond formation.

In the fourth spectra of TMS + P-123 + ADS, there were peaks observed at 2969, and 2867 cm^{-1} which stand for C-H stretching and O-H stretching respectively. The C=C stretching appearing at 1685 cm^{-1} of TMS now gets to a higher wavenumber of 1717 cm^{-1}. The C-N stretching of TMS from 1380 cm^{-1} is shifted to 1373 cm^{-1}. This is one shift to lower wavenumber. 1128 cm^{-1} of TMS is shifted to 1091 cm^{-1} with a very strong peak. This is a second shift to a lower wavenumber. The 1264 cm^{-1} C-O stretching is uniformly present in all four spectrums which means that this area is not affected by bonding. The 3566 cm^{-1} of N-H stretching area gets a medium signal which was not present in the TMS. Here also there is bond formation. Hence, in the complex of TMS + P-123 + ADS, there are three sites where bond formation is taking place.

Thus, looking at the structural changes occurring for TMS one can say that TMS + P-123 + ADS are bound more strongly with more binding sites than TMS + P-123 + CPB.

3.3. UV – Visible Spectroscopy:

In order to observe to change in hydrophobicity and complex formation occurring in TMS in the environment of the single and binary micellar solution, UV Spectroscopy was conducted. The methanolic aqueous solution of TMS was used for the purpose. It displayed the λ_{max} at 294 nm which is in good agreement with literature [61,62]. A calibration of TMS was constructed which is shown in Fig S1 of the supplementary section. There were three sets of readings taken to visualize the effect of anionic/cationic charge in the mixed micelle during interaction with TMS. They were P-123, P-123 + CPB and P-123 + ADS. The CPB solutions were sufficiently diluted (above CMC) before adding the drug solutions.

Journal of Chemical Health Risks

www.jchr.org

JCHR (2023) 13(5), 581-608 | ISSN:2251-6727

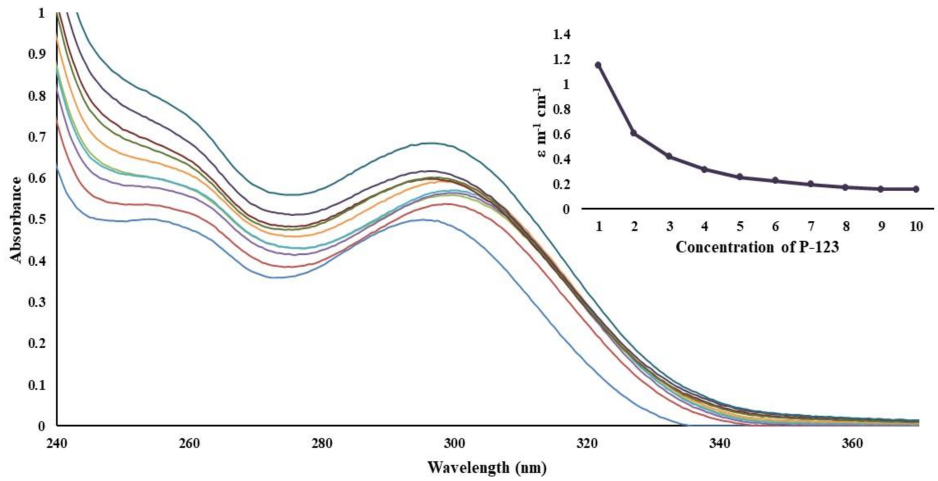

Fig 5 (a). UV absorbance spectrum of Telmisartan with different concentrations of Pluronic P-123 **(A).** X (14.41 μM) **(B).** X + P-123 (0.43 mM), **(C).** X + P-123 (0.87 mM), **(D).** X + P-123 (1.30 Mm), **(E).** X + P-123 (1.74 mM), **(F).** X + P-123 (2.17 mM), **(G).** X + P-123 (2.61 mM), **(H).** X + P-123 (3.05 mM), **(I).** X + P-123 (3.48 mM), **(J).** X + P-123 (3.92 mM). Inset: Molar extinction coefficient vs. concentration

In the first set, different concentrations of P-123 were added to the TMS solution. The spectra are shown in Fig 5 (a). It can be seen that there is a red shift in the λ_{max} by 4 nm with increased absorbance on the addition of nonionic P-123. This polymeric surfactant P-123 is an important pluronic that has the capacity to solubilize many hydrophobic drugs [63-68]. With TMS also it has been used earlier [18]. Because of its nontoxicity, it has been preferred in the solubilization of many drugs in the pharmaceutical field. To the aqueous solution of TMS, surfactant P-123 was added in the range of 0.43 mM to 3.92 mM. This concentration was chosen well above CMC to ensure complete micellization. The red shift and higher absorbance indicated that more drug molecules are getting solubilized in the micelles of P-123. The absorbance spectra 294 nm is due to π -π* transition. And there is a complex formation taking place between TMS and P-123. The inset shows the change in the extinction coefficient of the absorbance.

The next set of readings was taken for fixed (TMS 14.41 μM + P-123 0.43 mM) concentration with varied cationic surfactant CPB. The CPB concentration varied from 1.04 mM to 9.36 mM, which is above CMC. In the presence of this cationic mixed micellar solution, there was a 4.5 nm redshift with increased absorbance Fig 5 (b). This infers complex formation taking place in the mixed micellar solution. At high concentrations, however, the nature of the curve changed which may be due to a change in the micellar structure from spherical shape. The inset shows the change in the extinction coefficient trend of TMS while present in TMS + CPB mixture.

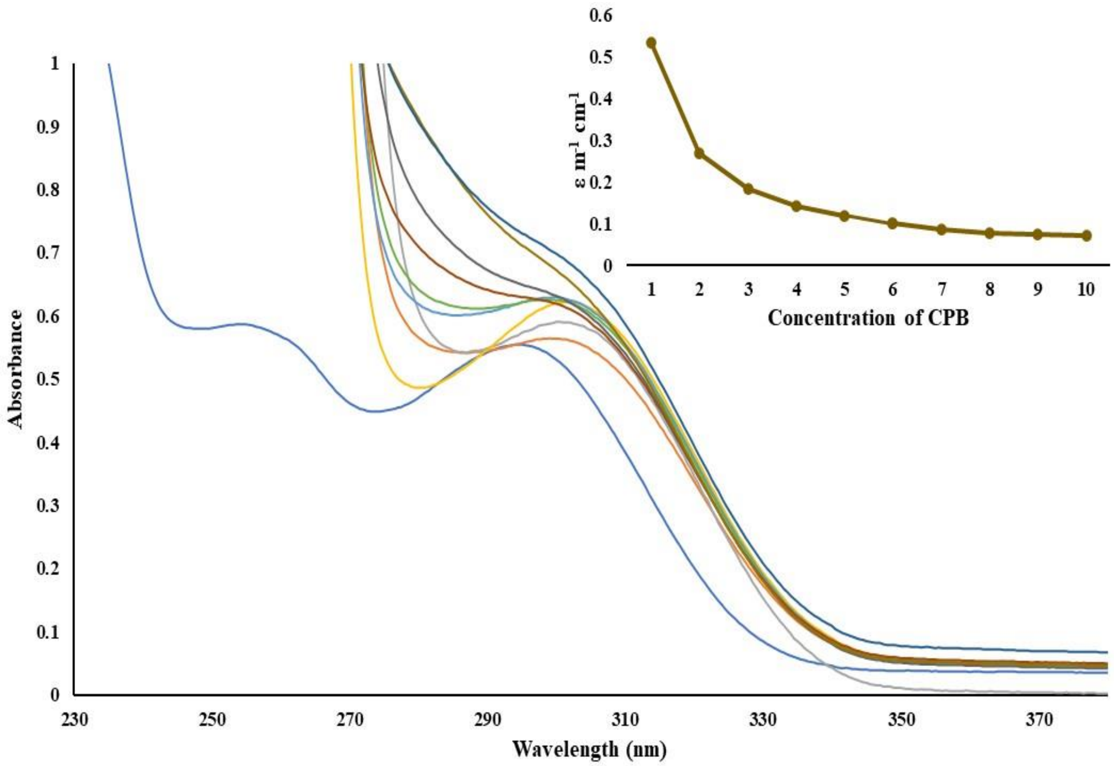

Fig 5 (b). UV absorbance spectrum of Telmisartan in the presence of fixed Pluronic P-123 + different concentrations of Cationic Surfactant CPB **(A)**. TMS (14.41 µM) **(B)**. (TMS (14.41 µM) + P-123 (0.87 mM)) X + CPB (1.04 mM), **(C)**. X + CPB (2.08 mM), **(D)**. X + CPB (3.12 mM), **(E)**. X + CPB (4.16 mM), **(F)**. X + CPB (5.20 mM), **(G)**. X + CPB (6.24 mM), **(H)**. X + CPB (7.28 mM), **(I)**. X + CPB (8.32 mM), **(J).** X + CPB (9.36 mM). Inset: Molar extinction coefficient vs. concentration.

The third set of spectra was recorded using fixed (TMS + P-123) concentration and varied ADS and is given in Fig 5 (c). The surfactant ADS was chosen in the 3.17 mM to 28.57 mM which were all above the CMC. In this case, also, the negative ion of ADS impacted the mixed micelle of P-123 + ADS while interacting with TMS. There was a 2.5 nm redshift with increased absorbance. These implied that there are more TMS molecules present in the mixed micellar solution. The inset displays the change in extinction coefficient of TMS in TMS + ADS mixture. From the absorbance values, a B-H plot was drawn to calculate the binding constant using the formula given in section 2.4. The results are displayed in Table 4.

Journal of Chemical Health Risks
www.jchr.org
JCHR (2023) 13(5), 581-608 | ISSN:2251-6727

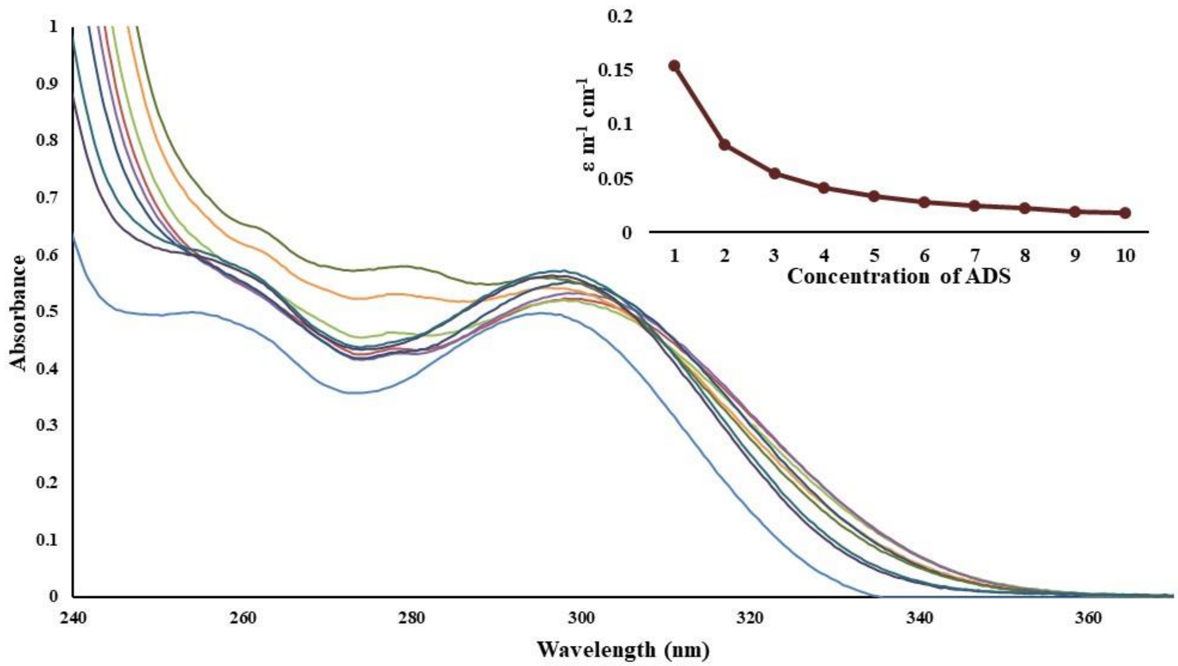

Fig 5 (c). UV absorbance spectrum of Telmisartan in the presence of fixed Pluronic P-123 + different concentrations of Anionic Surfactant ADS **(A).** TMS (14.41 µM) **(B).** (TMS (14.41 µM) + P-123 (0.87 mM)) X + ADS (3.17 mM), **(C).** X +DS (6.35 mM), **(D).** X + ADS (9.52 mM), **(E).** X + ADS (12.7 mM), **(F).** X + ADS (15.87 mM), **(G).** X + ADS (19.05 mM), **(H).** X + P-123 (0.87 mM) + ADS (22.22 mM), **(I).** X + ADS (25.4 mM), **(J).** X + ADS (28.57 mM). Inset: Molar extinction coefficient vs. concentration.

It is observed that the binding constant for a single polymeric surfactant P-123 was 79.36 M^{-1}. The values for P-123 + CPB and P-123 + ADS were 456.62 M^{-1} and 1138.78 M^{-1}, respectively. This indicates enhanced binding of the latter two combinations than the former. Hence, it can be said that in both the binary micellar mediums there is enhanced binding of TMS binding compared to the single P-123 surfactant.

Table 4. Evaluation of binding constant (K_b), and correlation coefficients (R_c) for complex from TMS + P-123, TMS + P-123 + CPB, TMS + P-123 + ADS Ultra Violet visible technique

system	K_b Binding constant m^{-1}	R_c Correlation coefficient
TMS + P-123	79.36 ± 8.651	0.9285 ± 0.123
TMS + P-123 + CPB	456.62 ± 3.078	0.9811 ± 0.355
TMS + P-123 + ADS	1133.78 ± 2.27	0.9699 ± 0.242

Journal of Chemical Health Risks
www.jchr.org
JCHR (2023) 13(5), 581-608 | ISSN:2251-6727

3.4. Zeta Potential Measurements:

To examine the electrochemical behavior of the three single and two mixed micellar solutions and the behavior of TMS in the mixed systems, a zeta potential (ZP) experiment was carried out [68-74]. The first aliquot was for P-123. The zeta potential was found to be 2.39 mV with mobility of 0.18 µm cms^{-1}. This low value of zeta and mobility is due to the nonionic nature of the surfactant. Pure ADS and pure CPB solutions displayed high negative and positive ZP values of -44.6 mV and 14.1 mV, respectively. As observed, ADS shows a greater effect on ZP which is in the stable colloidal range compared to CPB. The next couple of readings were taken for P-123 + CPB and P-123 + ADS. Here, the ZP value got increased for both due to the addition of nonionic P-123. The ZP was 25.8 mV, and 13.3 mV, and the mobility changed to 2.0 mV and -1.9 mV, respectively for CPB and ADS mixed micellar sets. The results are shown in Table 5 and Fig 6.

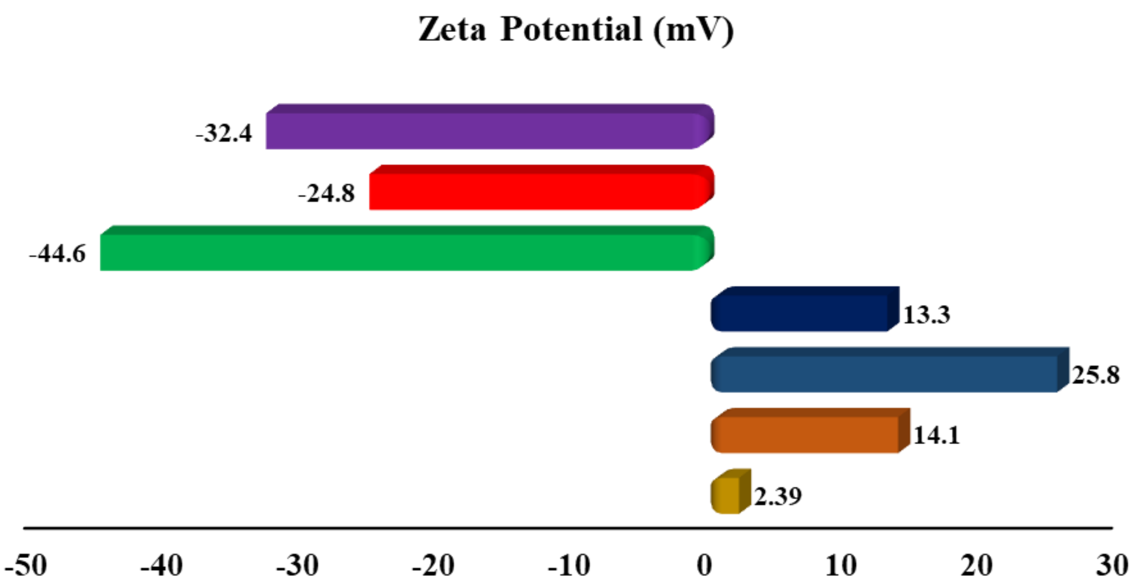

Fig 6. Change in the zeta potential of Drug Telmisartan in single and mixed micellar systems. (Assign which colour is for which system here itself or near the values.) (a). P-123, (b). CPB, (c). P-123+CPB, (d). P-123+CPB+TMS, (e). ADS, (f). P-123+ADS, (g). P-123+ADS+TMS

Table 5. Zeta potential for pure and mixed Pluronic in the presence and absence of Telmisartan.

Surfactant system	ZP (mV)	Mob (µm cm/Vs)
P-123	2.39 ± 0.764	0.18 ± 0.059
CPB	14.1 ± 1.13	1.105 ± 0.088
P-123 + CPB	25.8 ± 0.700	2.024 ± 0.052
P-123 + CPB + TMS	13.3 ± 2.30	1.044 ± 0.180
ADS	-44.6 ± 1.2	-3.496 ± 0.096
P-123 + ADS	-24.8 ± 0.651	-1.940 ± 0.051
P-123 + ADS + TMS	-32.4 ± 0.872	-2.540 ± 0.068

In the final step, TMS was added to both the mixed micellar systems wherein there was a change in the ZP and mobility. The CPB set changed from 25.8 mV to 13.3 mV and the ADS set from -24.8 mV to -32.4 mV. The value of ZP predicts that TMS in the mixed micellar medium produces stable colloidal particles mainly in ADS + P-123

Journal of Chemical Health Risks

www.jchr.org

JCHR (2023) 13(5), 581-608 | ISSN:2251-6727

micellar mixture with moderate mobility which is required for the drug to be mobile in the body.

3.5. DLS Measurements:

Drug-loaded micelles display different sizes than the normal micellar system. The sizes of single and binary micelles with and without TMS were measured through dynamic light scattering experiments. The two mixed micellar sets are presented separately in Fig 7 (a) and Fig 7 (b). The hydrodynamic diameter (Z_{ave}) values are shown in Table 6.

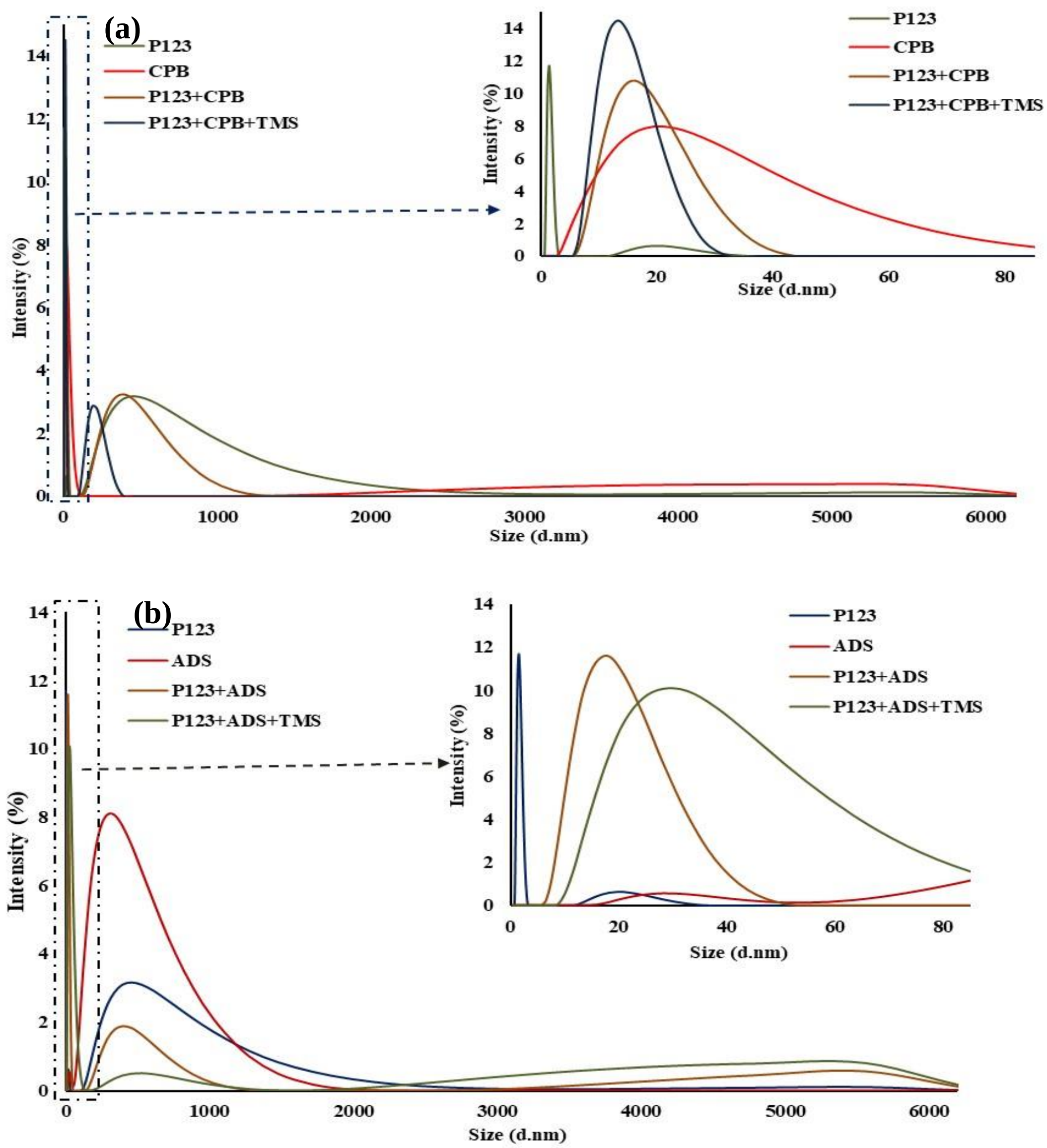

Fig 7. Dynamic light scattering data of Drug Telmisartan in single and mixed micellar **(a)** Cetyl Pyridinium Bromide and **(b)** Ammonium Dodecyl Sulfate systems.

Journal of Chemical Health Risks

www.jchr.org

JCHR (2023) 13(5), 581-608 | ISSN:2251-6727

Table 6. DLS data showing the variation of the hydrodynamic diameter in pure and mixed Pluronic in the presence and absence of Telmisartan.

Surfactant system	Z-Average (nm)	PDI
P-123	6.70 ± 0.231	0.525 ± 0.045
CPB	16.23 ± 0.965	0.331 ± 0.061
P-123 + CPB	18.74 ± 1.12	0.322 ± 0.048
P-123 + CPB + TMS	52.02 ± 4.062	0.145 ± 0.035
ADS	3.16 ± 0.335	0.247 ± 0.012
P-123 + ADS	17.26 ± 1.253	0.339 ± 0.621
P-123 + ADS + TMS	32.04 ± 0.541	0.228 ± 0.654

As observed, the size of single micelles of P-123, CPB, and ADS was observed to be 6.7, 16.23, and 3.1 nm respectively. The mixed micelles of P-123 + CPB and P-123 + ADS displayed a diameter of 18.74 and 17.26 nm respectively. On adding TMS to the mixed micelles, there was swelling of the micelle from 18.7 to 52.02 nm and 17.2 to 32.04 nm for CPB set and ADS set of mixed micelles respectively. This increase in the size of hydrodynamic diameter indicated that the mixed micelle has encapsulated more drug TMS molecules in the micellar cavity. The DLS of several micellar systems has been reported before [44,56,69-71,73,74]. The micellar size of ADS increases from 3.16 nm to 32.04 nm, which is a significant enhancement in size compared to CPB, which changes from 16.23 nm to 52.02 nm. Hence, it is apparent that P-123 + ADS can encapsulate more TMS molecules than P-123 + CPB.

In the administration of nanomedicines, it is observed that smaller particle sizes with less than 100 nm is favorable for tissue penetration and blood circulation [75-77]. In this case, both the polymeric-ionic binary combinations containing telmisartan with sizes 32.0 nm and 52.0 nm are suitable for cellular uptake.

3.6. SEM Measurements:

To visualize the surface morphology of the drug in a single/mixed micellar system, SEM photographs were taken. SEM images of TMS drugs in other chemical environments have been reported before in the literature [20,44,71,74].

The results are shown in Fig 8 (a), in Fig 8 (a) the particles of drug powder in different sizes and shapes with crystallinity are visible. In 1 μm the size looks magnified in the 500 nm figure without any change in geometrical shape. In addition to P-123 to TMS in Fig. 8(b), the gel nature of P-123 is reflected which is visible as capsule shapes in 1 μm and 500 nm resolution. There is a drastic change in the shape and appearance of particles suggesting that TMS is encapsulated in a polymeric micelle of P-123. On adding mixed micelle P-123 + CPB to TMS in Fig 8 (c) and P-123 + ADS to the drug in Fig 8 (d), the capsule-shaped drug looks to be somewhat homogenous with solid particles of capsule shape in both 1 μm and 500 nm resolution.

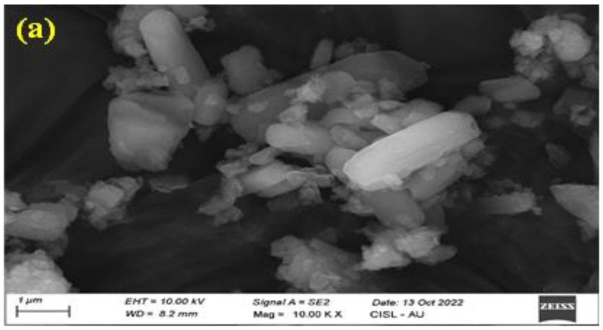

TMS (1 µm)

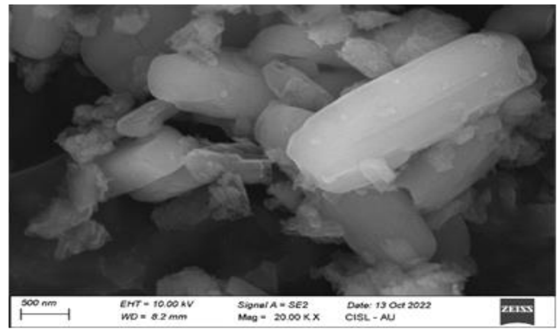

TMS (500 nm)

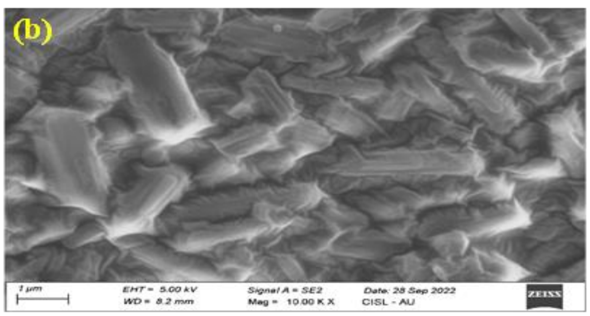

TMS +P-123 (1 µm)

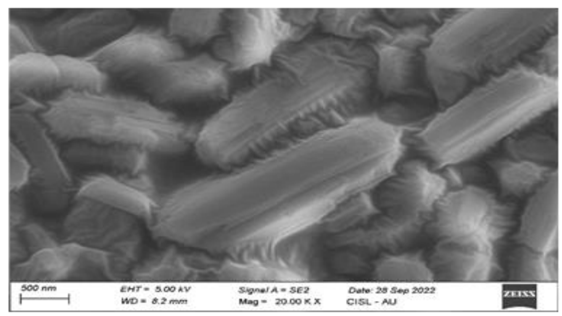

TMS +P-123 (500 nm)

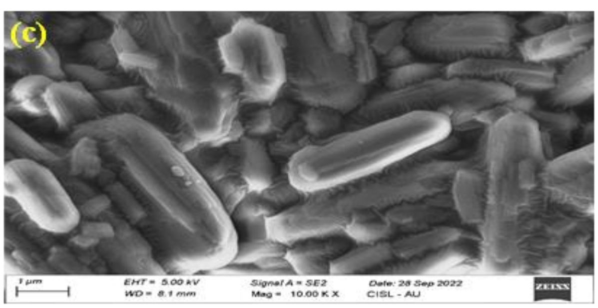

TMS +P-123 + CPB (1 µm)

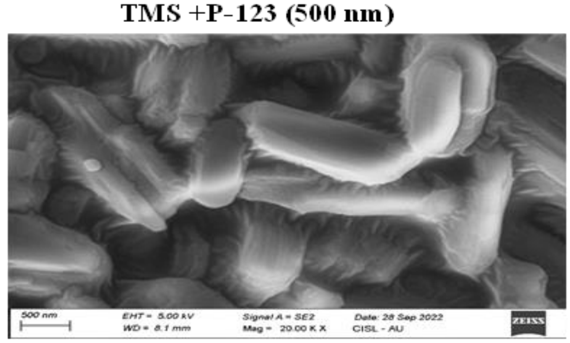

TMS +P-123 + CPB (500 nm)

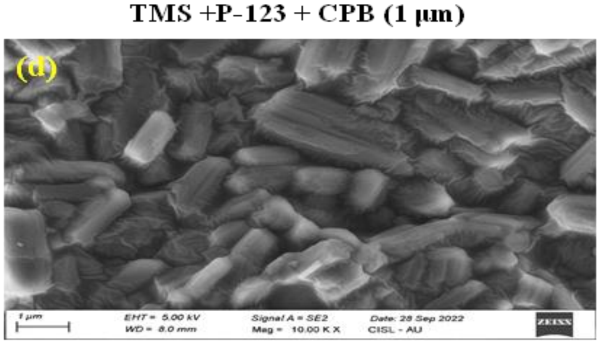

TMS +P-123 + ADS (1 µm)

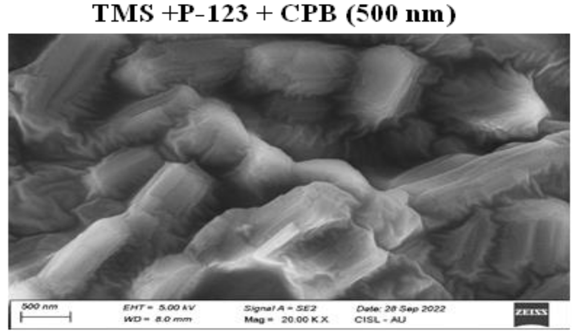

TMS +P-123 + ADS (500 nm)

Fig 8. SEM images of **(a).** TMS, **(b).** TMS + P-123, **(c).** TMS + P-123 + CPB, **(d).** TMS + P-123 + ADS at different magnification.

Conclusion:

Two polymeric binary micellar mediums are identified for solubilizing the anti-hypertensive drug TMS. The conductivity studies demonstrated spontaneity in micellization for the drug-encapsulated mixed micelles. The UV spectroscopy revealed a greater binding constant for TMS + P-123 + ADS and TMS + P-123 + CPB system compared to the single micelle of P-123. Furthermore, the former combination has more efficient binding than the latter, predicting ADS, a more suitable ionic surfactant in the polymeric binary micellar system for TMS. This was further affirmed by the particle size analysis by DLS studies and zeta potential analysis. The size of both polymeric-ionic binary combinations of TMS was 32.0 nm and 52.0 nm which is ideal for tissue penetration and blood circulation. The zeta potential measurement of TMS + P-123 + ADS shows -32.4 mV against TMS + P-123 + CPB value, 13.3 mV. This is indicative of a more stable colloidal system of the former combination. It is due to probable higher affinity of ADS than CPB while present in binary system while interacting with TMS. This report offers two alternate combinations of the binary polymeric surfactants of Telmisartan with higher solubilization, and better cellular uptake.

Compliance with ethical Standards

Conflict of interest

The authors state that they do not have any conflicts of interest.

Funding Information

The authors declare that they have no known competing financial interests or personal relationships that could have appeared to influence the work reported in this paper.

Credit authorship contribution statement

E. Paul Raj: Investigation, Methodology, Writing – original. **Dr. Sasmita Dash:** Supervision, Validation, Writing – review & editing. **Sutharsan karunanithi:** Conceptualization, Data curation, Formal analysis. **Puspalata Rajesh:** Resources, Visualization, Data curation, Formal analysis.

Data Availability

This published paper includes all data produced or analyzed during this project.

References:

[1] S. Zaza, S.M. Lucini, F. Sciascia, V. Ferrone, R. Cifelli, G. Carlucci, M. Locatelli, Recent advances in the separation and determination of impurities in pharmaceutical products, Instrum. Sci. Technol. **43,** 182–196 (2015). https://doi.org/10.1080/10739149.2014.921792.

[2] S. Stegemann, F. Leveiller, D. Franchi, H. de Jong, H. Lindén, When poor solubility becomes an issue: From early stage to proof of concept, Eur. J. Pharm. Sci. **31,** 249–261 (2007). https://doi.org/10.1016/j.ejps.2007.05.110.

[3] P.H.L. Tran, H.T.T. Tran, B.J. Lee, Modulation of microenvironmental pH and crystallinity of ionizable telmisartan using alkalizers in solid dispersions for controlled release, J. Control. Release. **129,** 59–65 (2008). https://doi.org/10.1016/j.jconrel.2008.04.001.

[4] H. Patil, R. V. Tiwari, M.A. Repka, Hot-Melt Extrusion: from Theory to Application in Pharmaceutical Formulation, AAPS PharmSciTech. **17,** 20–42 (2016). https://doi.org/10.1208/s12249-015-0360-7.

[5] B.R. Giri, J. Kwon, A.Q. Vo, A.M. Bhagurkar, S. Bandari, D.W. Kim, Hot-melt extruded amorphous solid dispersion for solubility, stability, and bioavailability enhancement of telmisartan, Pharmaceuticals. **14,** 1–18 (2021). https://doi.org/10.3390/ph14010073.

[6] Kolatkar. G, and E. Zisman, Pharmaceutical compositions of telmisartan. USA Patent, US20070116759A1, 2005., 2007.

[7] W. Wienen, M. Entzeroth, J.C.A. Van Meel, J. Stangier, U. Busch, T. Ebner, J. Schmid, H. Lehmann, K. Matzek, J. Kempthorne-Rawson, V. Gladigau, N.H. Hauel, A review on telmisartan: A novel, long-acting angiotensin II-receptor antagonist, Cardiovasc. Drug Rev. **18,** 127–154 (2000). https://doi.org/10.1111/j.1527-3466.2000.tb00039.x.

[8] B. Chatterjee, K.A.S. Al-Japairai, H.M. Alkhalidi, S. Mahmood, S.H. Almurisi, A.A. Doolaanea, T.A. Al-Sindi, Lyophilized amorphous dispersion of

telmisartan in a combined carrier‒alkalizer system: Formulation development and in vivo study, ACS Omega. **5,** 32466–32480 (2020). https://doi.org/10.1021/acsomega.0c04588.

[9] S. Kundu, N. Kumari, S.R. Soni, S. Ranjan, R. Kumar, A. Sharon, A. Ghosh, Enhanced Solubility of Telmisartan Phthalic Acid Cocrystals within the pH Range of a Systemic Absorption Site, ACS Omega. **3,** 15380–15388 (2018). https://doi.org/10.1021/acsomega.8b02144.

[10] R. Iyer, V.P. Jovanovska, K. Berginc, M. Jaklič, F. Fabiani, C. Harlacher, T. Huzjak, M.V. Sanchez-Felix, Amorphous solid dispersions (ASDs): The influence of material properties, manufacturing processes and analytical technologies in drug product development, Pharmaceutics. **13,** (2021). https://doi.org/10.3390/pharmaceutics13101682.

[11] M.A. Rub, D. Kumar, N. Azum, F. Khan, A.M. Asiri, Study of the interaction between promazine hydrochloride and surfactant (conventional/gemini) mixtures at different temperatures, J. Solution Chem. **43,** 930–949 (2014). https://doi.org/10.1007/s10953-014-0174-3.

[12] M. Maswal, A.H. Pandith, N. Islam, A.A. Dar, Co-solubilization of the hydrophobic drugs carbamazepine and nifedipine in aqueous nonionic surfactant media, J. Solution Chem. **42,** 1374–1392 (2013). https://doi.org/10.1007/s10953-013-0036-4.

[13] Y. Kadam, U. Yerramilli, A. Bahadur, Solubilization of poorly water-soluble drug carbamezapine in Pluronic® micelles: Effect of molecular characteristics, temperature and added salt on the solubilizing capacity, Colloids Surfaces B Biointerfaces. **72,** 141–147 (2009). https://doi.org/10.1016/j.colsurfb.2009.03.027.

[14] Z. Wei, J. Hao, S. Yuan, Y. Li, W. Juan, X. Sha, X. Fang, Paclitaxel-loaded Pluronic P123/F127 mixed polymeric micelles: Formulation, optimization and in vitro characterization, Int. J. Pharm. **376,** 176–185 (2009). https://doi.org/10.1016/j.ijpharm.2009.04.030.

[15] R.K. Das, N. Kasoju, U. Bora, Encapsulation of curcumin in alginate-chitosan-pluronic composite nanoparticles for delivery to cancer cells, Nanomedicine Nanotechnology, Biol. Med. **6,** 153–160 (2010). https://doi.org/10.1016/j.nano.2009.05.009.

[16] L.M. Han, J. Guo, L.J. Zhang, Q.S. Wang, X.L. Fang, Pharmacokinetics and biodistribution of polymeric micelles of paclitaxel with Pluronic P123, Acta Pharmacol. Sin. **27,** 747–753 (2006). https://doi.org/10.1111/j.1745-7254.2006.00340.x.

[17] Z. Liu, D. Liu, L. Wang, J. Zhang, N. Zhang, Docetaxel-Loaded pluronic P123 polymeric micelles: In vitro and in vivo evaluation, Int. J. Mol. Sci. **12,** 1684–1696 (2011). https://doi.org/10.3390/ijms12031684.

[18] M.E. Mohanty, V.J. Rao, A.K. Mishra, A fluorescence study on the interaction of telmisartan in triblock polymers pluronic P123 and F127, Spectrochim. Acta - Part A Mol. Biomol. Spectrosc. **121,** 330–338 (2014). https://doi.org/10.1016/j.saa.2013.09.122.

[19] Y. Zhang, Z. Zhi, T. Jiang, J. Zhang, Z. Wang, S. Wang, Spherical mesoporous silica nanoparticles for loading and release of the poorly water-soluble drug telmisartan, J. Control. Release. **145,** 257–263 (2010). https://doi.org/10.1016/j.jconrel.2010.04.029.

[20] Y. Zhang, T. Jiang, Q. Zhang, S. Wang, Inclusion of telmisartan in mesocellular foam nanoparticles: Drug loading and release property, Eur. J. Pharm. Biopharm. **76,** 17–23 (2010). https://doi.org/10.1016/j.ejpb.2010.05.010.

[21] Anirudh Srivastava, Hiromasa Uchiyama, Yuhei Wada, Yuta Hatanaka, Yoshiyuki Shirakawa, Kazunori Kadota, Yuichi Tozuka. "Mixed micelles of the antihistaminic cationic drug diphenhydramine hydrochloride with anionic and non-ionic surfactants show improved solubility, drug release and cytotoxicity of ethenzamide." J. Mol. Liq. **277,** 349-359 (2019).

[22] Anirudh Srivastava, Osvaldo Yañez, Plinio Cantero-López. "Mixed micellization of bile salts and transglycosylated stevia and enhanced binding and solubility of non-steroidal anti-inflammatory drugs

using mixed micelle." J. Mol. Liq. **311**, 113341 (2020).

[23] Mukul Kumar, Kavya Khushi, Anshika Bhardwaj, Debojit Kumar Deb, Nandini Singh, Daniyal Elahi, Simran Sharma, Gaurav Bajpai, Anirudh Srivastava,. "In-vitro study for Ibuprofen encapsulation, controlled release and cytotoxicity improvement using excipient-drugs mixed micelle."Colloids and Surfaces A: Physicochemical and Engineering Aspects **654,** 130057 (2022).

[24] Mukul Kumar, Vaishali Singh, Riya Choudhary, Debojit kumar deb , Sandeepika Singh , Anirudh Srivastava. "Mixed Micellization of drug-excipients and its application to enhance the binding and encapsulation efficacy of ibuprofen in aqueous media."Colloids and Surfaces A: Physicochemical and Engineering Aspects **628,** 127268 (2021).

[25] Z. Huang, S. Parikh, W.P. Fish, Interactions between a poorly soluble cationic drug and sodium dodecyl sulfate in dissolution medium and their impact on in vitro dissolution behavior, Int. J. Pharm. **535,** 350–359 (2018). https://doi.org/10.1016/j.ijpharm.2017.10.063.

[26] N.N.S. Mai, Y. Otsuka, Y. Kawano, T. Hanawa, Preparation and characterization of solid dispersions composed of curcumin, hydroxypropyl cellulose and/or sodium dodecyl sulfate by grinding with vibrational ball milling, Pharmaceuticals. **13,** 1–15 (2020). https://doi.org/10.3390/ph13110383.

[27] Anjali. S, Vigneshwari. R, K. Sivakumar, S. Dash, Effect of antidiabetic drug metformin hydrochloride on micellization behavior of cetylpyridinium bromide in aqueous solution, J. Biomol. Struct. Dyn. 1–14. https://doi.org/10.1080/07391102.2023.2249113.

[28] P. Alexandridis, J.F. Holzwarth, T.A. Hatton, Micellization of Poly(ethylene oxide)-Poly(propylene oxide)-Poly(ethylene oxide) Triblock Copolymers in Aqueous Solutions: Thermodynamics of Copolymer Association, Macromolecules. **27,** 2414–2425 (1994). https://doi.org/10.1021/ma00087a009.

[29] I. Goldmints, F.K. Von Gottberg, K.A. Smith, T.A. Hatton, Small-angle neutron scattering study of PEO-PPO-PEO micelle structure in the unimer-to-micelle transition region, Langmuir. **13,** 3659–3664 (1997). https://doi.org/10.1021/la970140v.

[30] Z.A. Al-anber, Thermodynamic studies of interaction between cetylpyridinium bromide and lysozyme by means of calorimetric titrations, J. Therm. Anal. Color. **111,** 823–830 (2012). https://doi.org/10.1007/s10973-011-2146-9.

[31] J.J. Chung, S.W. Lee, J.H. Choi, Salt Effects on the Critical Micelle Concentration and Counterion Binding of Cetylpyridinium Bromide Micelles, Bull. Korean Chem. Soc. **12,** 411–413 (1991). https://doi.org/10.5012/bkcs.1991.12.4.411.

[32] L.R. Harutyunyan, S.A. Markarian, Effect of dimethylsulfoxide and diethylsulfoxide on micellization and viscometric properties of cetylpyridinium bromide aqueous solutions, J. Mol. Liq. **160,** 136–139 (2011). https://doi.org/10.1016/j.molliq.2011.03.010.

[33] Y.G. Devi, J. Gurung, A.K. Pulikkal, Micellar Solution Behavior of Cetylpyridinium Surfactants in 2-Propanol-Water Mixed Media at Different Temperatures, J. Chem. Eng. Data. **66,** 368–378 (2021). https://doi.org/10.1021/acs.jced.0c00734.

[34] K. Kang, H. Kim, K. Lim, Effect of temperature on critical micelle concentration and thermodynamic potentials of micellization of anionic ammonium dodecyl sulfate and cationic octadecyl trimethyl ammonium chloride, Colloids Surfaces A. **189,** 113–121 (2001). https://doi.org/10.1016/S0927-7757(01)00577-5.

[35] K. Kang, H. Kim, K. Lim, N. Jeong, Mixed Micellization of Anionic Ammonium Dodecyl Sulfate and Cationic Octadecyl Trimethyl Ammonium Chloride, Bull. Korean Chem. Soc. **22,** 1009–1014 (2001). https://doi.org/10.5012/bkcs.2001.22.9.1009.

[36] A. Packter, M. Donbrow, the Critical Micelle Concentrations of Double Long-Chain Electrolytes (Amine Soaps) in Aqueous Solution, J. Pharm. Pharmacol. **15,** 317–324 (1963).

https://doi.org/10.1111/j.2042-7158.1963.tb12788.x.

[37] H. Kim, K. Lim, A model on the temperature dependence of critical micelle concentration, Colloids Surfaces A. **235,** 121–128 (2004). https://doi.org/10.1016/j.colsurfa.2003.12.019.

[38] H.U. Kim, K.H. Lim, Sizes and structures of micelles of cationic octadecyl trimethyl ammonium chloride and anionic ammonium dodecyl sulfate surfactants in aqueous solutions, Bull. Korean Chem. Soc. **25,** 382–388 (2004). https://doi.org/10.5012/bkcs.2004.25.3.382.

[39] O. Greksáková, J. Oremusová, M. Vojteková, F. Kopecký, SSpectrophotometric Study of the Effect of Univalent Electrolytes on Critical Micelle Concentrations of [1 -(Ethoxycarbonyl)pentadecyl]trimethylammonium, 1-Hexadecylpyridinium, and Dimethylbenzyldodecylammonium Bromides, Chem. Pap. **48,** 300–305 (1994).

[40] M. Vojteková, F. Kopecký, O. Greksáková, J. Oremusová, Effect of Addition of KX Type Electrolytes and Temperature on the Critical Micellar Concentrations of 1-Cetylpyridinium and Carbethopendecinium Bromides, Collect. Czechoslov. Chem. Commun. **59,** 99–105 (1994). https://doi.org/10.1135/cccc19940099.

[41] P. Karunanithi, R. Vigneshwari, S. Dash, Physicochemical properties of piroxicam in ionic-mixed micellar medium: effect of charge on the micellization behaviour, Colloid Polym. Sci. **300,** 1355–1368 (2022). https://doi.org/10.1007/s00396-022-05027-4.

[42]. M. Jangde, S.K. Chatterjee, M. Jain, S. Ghosh, R. Jangde, D. Sinha, The Effect of Temperature on the Critical Micelle Concentration and Micellar Solubilization of Poorly Water Soluble Drugs, Biosci. Biotechnol. Res. Asia. **19,** 1045–1050 (2022). https://doi.org/10.13005/bbra/3054.

[43] C. Muankaew, P. Jansook, H.H. Sigurcrossed D Signsson, T. Loftsson, Cyclodextrin-based telmisartan ophthalmic suspension: Formulation development for water-insoluble drugs, Int. J. Pharm. **507,** 21–31 (2016). https://doi.org/10.1016/j.ijpharm.2016.04.071.

[44] C. Sharma, M.A. Desai, S.R. Patel, Effect of surfactants and polymers on morphology and particle size of telmisartan in ultrasound-assisted anti-solvent crystallization, Chem. Pap. **73,** 1685–1694 (2019). https://doi.org/10.1007/s11696-019-00720-1.

[45] L.Y. Chin, J.Y.P. Tan, H. Choudhury, M. Pandey, S.P. Sisinthy, B. Gorain, Development and optimization of chitosan coated nanoemulgel of telmisartan for intranasal delivery: A comparative study, J. Drug Deliv. Sci. Technol. **62,** 102341 (2021). https://doi.org/10.1016/j.jddst.2021.102341.

[46] R. Kumar, G.C. Soni, S.K. Prajapati, Formulation development and evaluation of Telmisartan Nanoemulsion, Int. J. Res. Dev. Pharm. Life Sci. **6,** 2711–2719 (2017). https://doi.org/10.21276/ijrdpl.2278-0238.2017.6(4).2711-2719.

[47] M.S. Reddy, B. Rambabu, K.A. Vijetha, Development and Evaluation of Solid Self Nano Emulsifying Drug, Int. J. Pharm. Sci. Res. **9,** 3398–3407 (2018). https://doi.org/10.13040/IJPSR.0975-8232.8(9).3948-61.

[48] R.L. Mhetre, V.B. Hol, R. Chanshetty, S.N. Dhole, Tailoring of Antihypertensive Drug-Loaded Nanoparticles: In Vitro, Toxicity, and Bioavailability Assessment, Bionanoscience. **12,** 28–40 (2022). https://doi.org/10.1007/s12668-021-00910-w.

[49] N. Chella, N. Narra, T. Rama Rao, Preparation and Characterization of Liquisolid Compacts for Improved Dissolution of Telmisartan, J. Drug Deliv. **2014,** 1–10 (2014). https://doi.org/10.1155/2014/692793.

[50] X. Shi, T. Xu, W. Huang, B. Fan, X. Sheng, Stability and Bioavailability Enhancement of Telmisartan Ternary Solid Dispersions: the Synergistic Effect of Polymers and Drug-Polymer(s) Interactions, AAPS PharmSciTech. **20,** 1–13 (2019). https://doi.org/10.1208/s12249-019-1358-3.

[51] P.A.A. Borba, M. Pinotti, G.R.S. Andrade, N.B. Da Costa, L.R. Olchanheski, D. Fernandes, C.E.M. De Campos, H.K. Stulzer, The effect of mechanical grinding on the formation, crystalline changes and dissolution behaviour of the inclusion complex of telmisartan and β-cyclodextrins, Carbohydr. Polym. **133,** 373–383 (2015). https://doi.org/10.1016/j.carbpol.2015.06.098.

[52] Y. Cao, L.L. Shi, Q.R. Cao, M.S. Yang, J.H. Cui, In-vitro characterization and oral bioavailability of organic solvent-free solid dispersions containing telmisartan, Iran. J. Pharm. Res. **15,** 385–394 (2016).

[53] M. Ganesh, U. Ubaidulla, G. Rathnam, H.T. Jang, Chitosan-telmisartan polymeric cocrystals for improving oral absorption: In vitro and in vivo evaluation, Int. J. Biol. Macromol. **131,** 879–885 (2019). https://doi.org/10.1016/j.ijbiomac.2019.03.141.

[54] R.A. Aldeeb, M.F. El-Miligi, M. El-Nabarawi, R. Tag, H.M.S. Amin, A.A. Taha, Enhancement of the Solubility and Dissolution Rate of Telmisartan by Surface Solid Dispersions Employing Superdisintegrants, Hydrophilic Polymers and Combined Carriers, Sci. Pharm. **90,** 71 (2022). https://doi.org/10.3390/scipharm90040071.

[55] A.M. Rashid, M.Y. Ismail, L.H. Samein, Solubility and dissolution rate enhancement of poorly water soluble telmisartan by melt granulation technique using soluplus and PEG8000 as carrier, Int. J. Pharm. Res. **12,** 1203–1209 (2020). https://doi.org/10.31838/ijpr/2020.SP1.194.

[56] K.J. Hasson, M.M. Ghareeb, Long term stability and in-vitro release study of telmisartan complex included by hydroxypropyl-beta-cyclodextrin in directly compressed tablet using ion-pair reversed phase high-performance liquid chromatography, Int. J. Drug Deliv. Technol. **11,** 974–979 (2021). https://doi.org/10.25258/ijddt.11.3.54.

[57] P. Shrimal, G. Jadeja, J. Naik, S. Patel, Continuous microchannel precipitation to enhance the solubility of telmisartan with poloxamer 407 using Box-Behnken design approach, J. Drug Deliv. Sci. Technol. **53,** 101225 (2019). https://doi.org/10.1016/j.jddst.2019.101225.

[58] X. Shi, X. Zhou, S. Shen, Q. Chen, S. Song, C. Gu, C. Wang, Improved in vitro and in vivo properties of telmisartan in the co-amorphous system with hydrochlorothiazide: A potential drug-drug interaction mechanism prediction, Eur. J. Pharm. Sci. **161,** 105773 (2021). https://doi.org/10.1016/j.ejps.2021.105773.

[59] A. Almotairy, M. Almutairi, A. Althobaiti, M. Alyahya, S. Sarabu, A. Alzahrani, F. Zhang, S. Bandari, M.A. Repka, Effect of pH modifiers on the solubility, dissolution rate, and stability of telmisartan solid dispersions produced by hot-melt extrusion technology, J. Drug Deliv. Sci. Technol. **65,** 102674 (2021). https://doi.org/10.1016/j.jddst.2021.102674.

[60] A. Chandra, M.V. Ghate, K.S. Aithal, S.A. Lewis, In silico prediction coupled with in vitro experiments and absorption modeling to study the inclusion complex of telmisartan with modified beta-cyclodextrin, J. Incl. Phenom. Macrocycl. Chem. **91,** 47–60 (2018). https://doi.org/10.1007/s10847-018-0797-x.

[61] M.H. Teaima, M. Yasser, M.A. El-Nabarawi, D.A. Helal, Proniosomal telmisartan tablets: Formulation, in vitro evaluation and in vivo comparative pharmacokinetic study in rabbits, Drug Des. Devel. Ther. **14,** 1319–1331 (2020). https://doi.org/10.2147/DDDT.S245013.

[62] F. Sánchez Rojas, C. Bosch Ojeda, Recent development in derivative ultraviolet/visible absorption spectrophotometry: 2004-2008. A review, Anal. Chim. Acta. **635,** 22–44 (2009). https://doi.org/10.1016/j.aca.2008.12.039.

[63] L.F. Gonçalves, C. Fernandes-Santos, Telmisartan detection by UV spectrophotometry in mice drinking water, Anal. Sci. Adv. **2,** 408–415 (2021). https://doi.org/10.1002/ansa.202000111.

[64] N. Patel, J.K. Patel, Analytical methodologies for determination of telmisartan: An overview, Int. J. Pharm. Pharm. Sci. **5,** 17–22 (2013). https://doi.org/10.20959/wjpps20179-10024.

[65] K. Patel, K. Dhudasia, A. Patel, J. Dave, C. Patel, Stress degradation studies on Telmisartan and development of a validated method by UV spectrophotometry in bulk and pharmaceutical dosage forms, Pharm. Methods. **2,** 253–259 (2011). https://doi.org/10.4103/2229-4708.93396.

[66] K. Ilango, P.S. Shiji Kumar, Validated spectrophotometric methods for the simultaneous determination of telmisartan and atorvastatin in bulk and tablets, Pharm. Methods. 3 112–116 (2012). https://doi.org/10.4103/2229-4708.103892.

[67] K.K. Pradhan, U.S. Mishra, A. Sahoo, K.C. Sahu, D. Mishra, R. Dash, Method development and validation of Telmisartan in bulk and pharmaceutical dosage forms by UV Spectrophotometric method, Int. J. Res. Pharm. Sci**.** **2,** 526–530 (2011).

[68] M. Rao, A. Bajaj, I. Khole, G. Munjapara, F. Trotta, In vitro and in vivo evaluation of β-cyclodextrin-based nanosponges of telmisartan, J. Incl. Phenom. Macrocycl. Chem. **77,** 135–145 (2013). https://doi.org/10.1007/s10847-012-0224-7.

[69] J. Patel, A. Dhingani, K. Garala, M. Raval, N. Sheth, Design and development of solid nanoparticulate dosage forms of telmisartan for bioavailability enhancement by integration of experimental design and principal component analysis, Powder Technol. **258,** 331–343 (2014). https://doi.org/10.1016/j.powtec.2014.03.001.

[70] J. Ahmad, K. Kohli, S.R. Mir, S. Amin, Formulation of self-nanoemulsifying drug delivery system for telmisartan with improved dissolution and oral bioavailability, J. Dispers. Sci. Technol. **32,** 958–968 (2011). https://doi.org/10.1080/01932691.2010.488511.

[71] C. Thapa, A. Ahad, M. Aqil, S.S. Imam, Y. Sultana, Formulation and optimization of nanostructured lipid carriers to enhance oral bioavailability of telmisartan using Box–Behnken design, J. Drug Deliv. Sci. Technol. **44,** 431–439 (2018). https://doi.org/10.1016/j.jddst.2018.02.003.

[72] J. Patel, G. Kevin, A. Patel, M. Raval, N. Sheth, Design and development of a self-nanoemulsifying drug delivery system for telmisartan for oral drug delivery, Int. J. Pharm. Investig. **1,** 112 (2011). https://doi.org/10.4103/2230-973x.82431.

[73] A. Bajaj, M.R.P. Rao, A. Pardeshi, D. Sali, Nanocrystallization by evaporative antisolvent technique for solubility and bioavailability enhancement of telmisartan, AAPS PharmSciTech. **13,** 1331–1340 (2012). https://doi.org/10.1208/s12249-012-9860-x.

[74] B.D. Bhagwat, J.I. D'Souza, Development of solid self micro emulsifying drug delivery system with neusilin US2 for enhanced dissolution rate of telmisartan, Int. J. Drug Dev. Res. **4,** 398–407 (2012).

[75] D.E. Owens, N.A. Peppas, Opsonization, biodistribution, and pharmacokinetics of polymeric nanoparticles, Int. J. Pharm. **307,** 93–102, (2006). https://doi.org/10.1016/j.ijpharm.2005.10.010.

[76] F. Alexis, E. Pridgen, L.K. Molnar, O.C. Farokhzad, reviews Factors Affecting the Clearance and Biodistribution of Polymeric Nanoparticles, Mol. Pharm. **5,** 505–515, (2008).

[77] A.J.M.J.F. Megan E. Fox, Francis C. Szoka, Soluble polymer carriers for the treatment of cancer: The importance of molecular architecture, Acc. Chem. Res. **42**, 1141–1151, (2009). https://doi.org/10.1021/ar900035f.

Journal of Chemical Health Risks

www.jchr.org

JCHR (2023) 13(5), 581-608 | ISSN:2251-6727

Figures and Tables Caption:

Fig 1. The structures of **(a)** drug Telmisartan **(b)** Pluronic P-123 **(c)** Cetyl Pyridinium Bromide and **(d)** Ammonium Dodecyl Sulfate.

Fig 2. Specific conductivity of **(a)** CPB **(b)** CPB + Pluronic P-123 and **(c)** CPB + Pluronic P-123 + Telmisartan

Fig 3. Specific conductivity of **(a)** ADS **(b)** ADS + Pluronic P-123 and **(c).** ADS + Pluronic P-123 + Telmisartan.

Fig 4. IR spectra of **(a).** TMS, **(b)**. TMS + P-123, **(c).** TMS + P-123 + CPB, **(d).** TMS + P-123 + ADS

Fig 5 (a). UV absorbance spectrum of Telmisartan with different concentrations of Pluronic P-123 **(A).** X (14.41 μM) **(B).** X + P-123 (0.43 mM), **(C).** X + P-123 (0.87 mM), **(D).** X + P-123 (1.30 Mm), **(E).** X + P-123 (1.74 mM), **(F).** X + P-123 (2.17 mM), **(G).** X + P-123 (2.61 mM), **(H).** X + P-123 (3.05 mM), **(I).** X + P-123 (3.48 mM), **(J).** X + P-123 (3.92 mM). Inset: Molar extinction coefficient vs. concentration.

Fig 5 (b). UV absorbance spectrum of Telmisartan in the presence of fixed Pluronic P-123 + different concentrations of Cationic Surfactant CPB **(A)**. TMS (14.41 μM) **(B)**. (TMS (14.41 μM) + P-123 (0.87 mM)) X + CPB (1.04 mM), **(C)**. X + CPB (2.08 mM), **(D)**. X + CPB (3.12 mM), **(E)**. X + CPB (4.16 mM), **(F)**. X + CPB (5.20 mM), **(G)**. X + CPB (6.24 mM), **(H)**. X + CPB (7.28 mM), **(I)**. X + CPB (8.32 mM), **(J).** X + CPB (9.36 mM). Inset: Molar extinction coefficient vs. concentration.

Fig 5 (c). UV absorbance spectrum of Telmisartan in the presence of fixed Pluronic P-123 + different concentrations of Anionic Surfactant ADS **(A).** TMS (14.41 μM) **(B).** (TMS (14.41 μM) + P-123 (0.87 mM)) X + ADS (3.17 mM), **(C).** X +ADS (6.35 mM), **(D).** X + ADS (9.52 mM), **(E).** X + ADS (12.7 mM), **(F).** X + ADS (15.87 mM), **(G).** X + ADS (19.05 mM), **(H).** X + P-123 (0.87 mM) + ADS (22.22 mM), **(I).** X + ADS (25.4 mM), **(J).** X + ADS (28.57 mM). Inset: Molar extinction coefficient vs. concentration.

Fig 6. Change in the zeta potential of Drug Telmisartan in single and mixed micellar systems. (Assign which colour is for which system here itself or near the values.) (a). P-123, (b). CPB, (c). P-123+CPB, (d). P-123+CPB+TMS, (e). ADS, (f). P-123+ADS, (g). P-123+ADS+TMS.

Fig 7. Dynamic light scattering data of Drug Telmisartan in single and mixed micellar (a) Cetyl Pyridinium Bromide and (b) Ammonium Dodecyl Sulfate systems.

Fig 8. SEM images of **(a).** TMS, **(b),** TMS + P-123, **(c).** TMS + P-123 + CPB, **(d).** TMS + P-123 + ADS at different magnifications.

Table 1. Thermodynamic parameters of Telmisartan in the ionic and non-ionic mixed micellar systems at different chemical environments were collected from literature with results from this work.

Table 2. The IR spectrum of **(i)** TMS, **(ii)** TMS + P-123, **(iii)** TMS +P-123 + ADS, **(iv)** TMS + P-123 + CPB.

Table 3. IR spectra of Telmisartan in different chemical environments collected from the literature.

Table 4. Evaluated binding constant (K_b), and correlation coefficients (R_c) for complex from TMS + P-123, TMS + P-123 + CPB, TMS + P-123 + ADS Ultra Violet visible technique.

Table 5. Zeta potential for pure and mixed Pluronic in the presence and absence of Telmisartan.

Table 6. DLS data showing the variation of the hydrodynamic diameter in pure and mixed Pluronic in the presence and absence of Telmisartan.

Supplementary Fig 1. Calibration of telmisartan.

Supplementary Fig 2. Evaluation of binding constant for complex from **(a).** TMS + P-123, **(b).** TMS + P-123 + CPB, **(c).** TMS + P-123 + ADS Ultra Violet visible technique.

Journal of Chemical Health Risks

www.jchr.org

JCHR (2023) 13(5), 581-608 | ISSN:2251-6727

Graphical Abstract

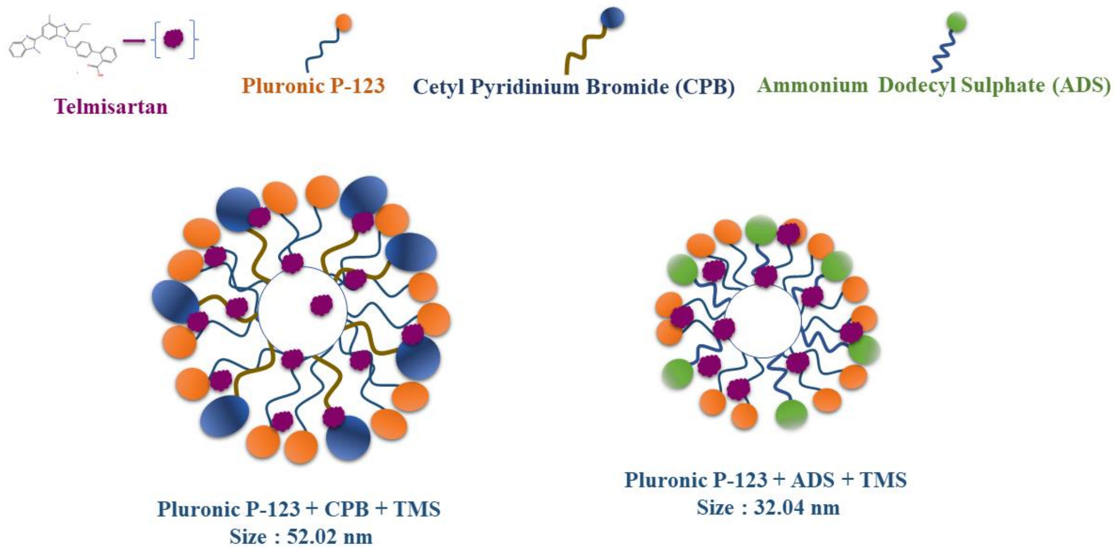

Journal of Chemical Health Risks

www.jchr.org

JCHR (2023) 13(5), 581-608 | ISSN:2251-6727

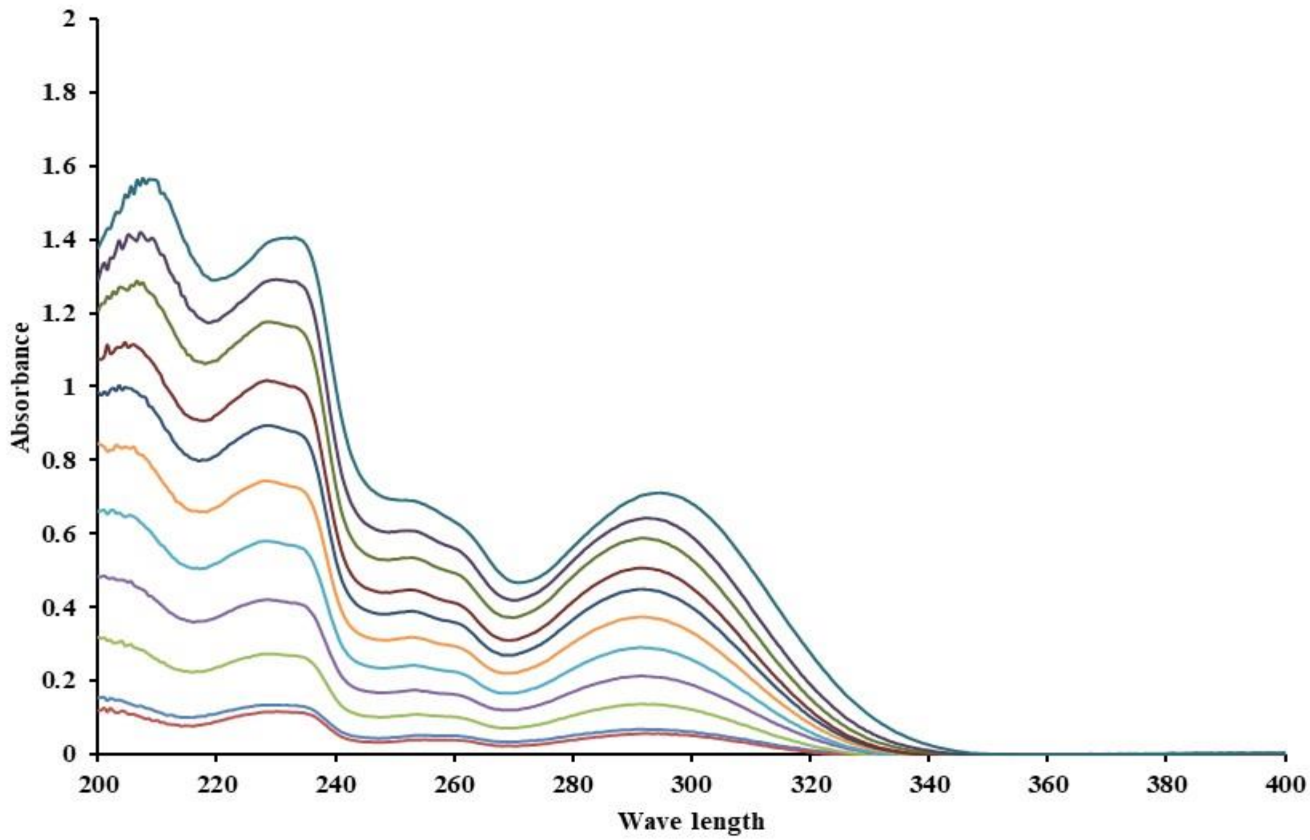

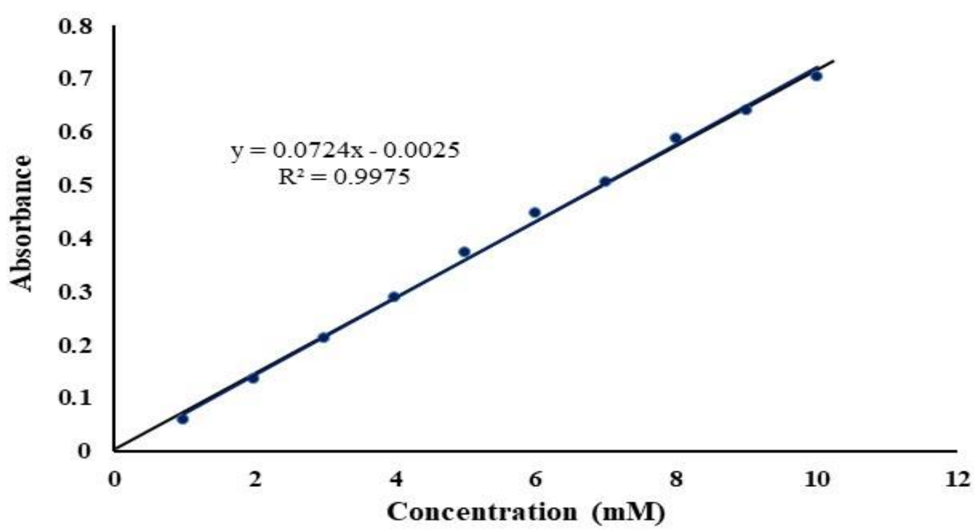

Supplementary Fig 1. Calibration of telmisartan

Journal of Chemical Health Risks

www.jchr.org

JCHR (2023) 13(5), 581-608 | ISSN:2251-6727

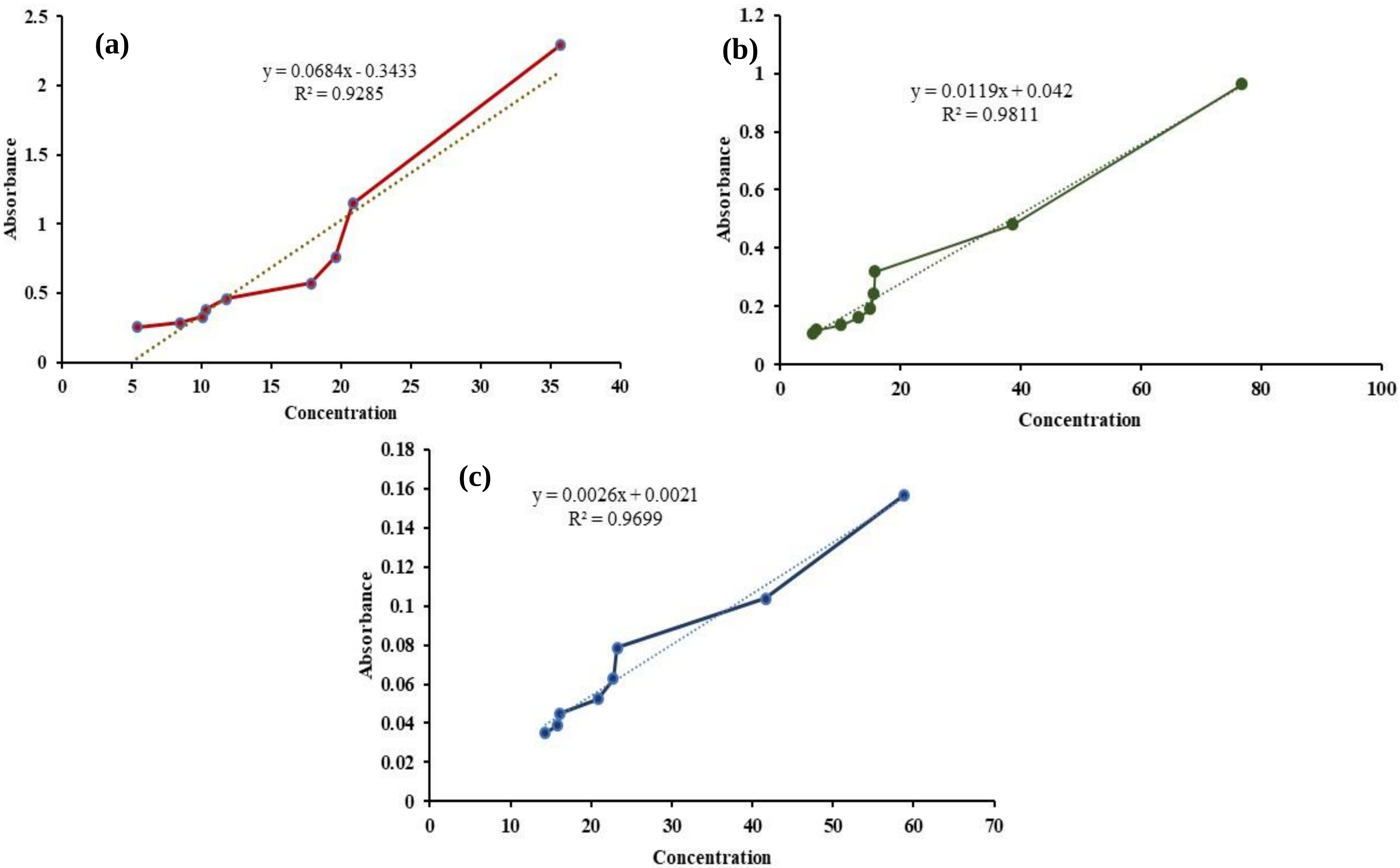

Supplementary Fig 2. Evaluation of binding constant for complex from **(a).** TMS + P-123, **(b).** TMS + P-123 + CPB, **(c).** TMS + P-123 + ADS Ultra Violet visible technique